Submitted to Physical Review D

E221
FERMILAB-PUB-78-107-E

The Mass Spectrum of Proton-Proton Inelastic Interactions from 55 to 400 GeV/c at Small Momentum Transfer *

R.D. Schamberger, Jr., J. Lee-Franzini, R. McCarthy

State University of New York at Stony Brook
Stony Brook, New York 11790

and

S. Childress, P. Franzini

Columbia University, New York, New York 10027

---

* Research supported in part by the National Science Foundation.

ABSTRACT

The doubly differential cross section $\frac{d^2\sigma}{dtdM^2}$ for the reaction $p+p \rightarrow p+X$ was measured as a function of the four momentum transfer squared (t), the missing mass squared (M^2), and the total center of mass energy squared (s). We covered the region $0.024 < -t < 0.234\,(\mathrm{GeV/c})^2$, $0 < M^2 < 0.12\ s\,(\mathrm{GeV})^2$, and $105 < s < 752\,(\mathrm{GeV})^2$, by detecting the slow recoil proton at large angles with solid state detectors. The data were taken on polypropelene $(CH_2)_n$ and carbon targets, and a subtraction was made to obtain the free proton cross section. We find that our differential cross section can be simply represented by:

$$d\sigma(s)/dM^2 = (15\pm0.5)/s + (2.9\pm0.1)/M^{3.7\pm0.1}\,\mathrm{mb/GeV}^2 .$$

The energy independent part of this result is identified

with the inelastic diffractive process for which we obtain $\sigma_{diff} = 3.6 \pm 0.4$ mb after doubling for p-p symmetry. We also observe no significant increase with s for the inclusive cross section integrated to 0.06s or 0.1s.

I. INTRODUCTION

The inclusive reaction $p+p \rightarrow p+X$ was studied versus energy at the Internal Target Area of Fermilab by interacting the proton beam during both the accelerating cycle and the coasting time, on polypropene ($(CH_2)_n$) and carbon fibers, and obtaining the free-proton cross section by subtraction. For an inclusive reaction, only three kinematical variables need to be defined. One variable, the total energy squared in the center of mass, was known by a knowledge of the magnetic field in the Main Ring Magnets (to $\pm$ 1%). The other two variables were defined by measuring in the laboratory the kinetic energy T and scattering angle θ of each detected slow recoil proton. From these variables, the usual Lorentz invariant variables, M^2, the total energy squared of X in its center of mass, and t, the four momentum transfer from the target to the recoil proton, can be calculated. We therefore measure the doubly differential yield $d^2N/dtdM^2$, which with appropriate normalization, results in absolute measurements of the inelastic cross sections, $d\sigma/dtdM^2$.

The cross sections $d\sigma/dtdM^2$ were measured over the range in t and M^2 of: $0.024 < |t| < 0.234 (GeV/c)^2$, $M^2 < 0.12\ s\ GeV^2$, at 7 discrete $\langle s \rangle$ values from 114 to 741 GeV^2, corresponding to laboratory beam energies from 55 to 400 GeV.

This study was partly motivated by the following questions: 1) Diffraction Dissociation - The possibility of observing diffractive inelastic processes producing states X of large

mass was first pointed out by Good and Walker in 1960.[1] We are interested here in determining whether this process can be unambiguously separated from the general inelastic cross section by identifying a contribution to the inelastic cross section which is energy independent. Another important property of the inelastic diffraction is the shape of the mass spectrum for which some models make explicit predictions.[2]

2) Rising Total Cross Section - This phenomenon, observed at both ISR[3] and Fermilab[4], is still in need of an explanation. Both theoretical[5] and experimental[6] claims have been made to the effect that this rise is all due to a rise of the inelastic diffractive cross section. This would imply that the diffractive cross section should rise by over 1 mb over our energy range.[7]

3) Scaling Contribution to the Inclusive Cross Section - There is considerable interest[8] in the magnitude as well as the M^2 dependence of a Feynman scaling contribution to the inclusive cross section.

4) The Relative Magnitudes of the Elastic, Diffractive and Total Cross Sections - In 1973, Pumplin[9] derived a unitarity bound limiting the diffractive cross section to be less than one-half of the total cross section minus the elastic cross section. This experiment measures simultaneously the elastic and diffractive cross section, yielding information on how saturated is the Pumplin Bound.

Our results can be summarized as follows:

a) The inclusive cross section, integrated over t and up to a constant fraction of available phase space in M^2 (i.e., up to a constant fraction of s) is independent of s to a few percent. A typical value is $\sigma_{inc}(M^2 < 0.1s) = 3.3$ mb.

b) The measured inclusive cross section integrated over our t range appears to be composed of two terms, the first term is energy independent, i.e. $d\sigma/dM^2)_I \sim f(M^2)$ and the second term scales with energy, i.e. $d\sigma/dM^2)_{II} \sim (s^{-1})g(M^2)$.

c) Specifically, all our data are well represented by the empirical formula $d\sigma/dM^2 = 15/s + 2.9\ M^{3.7}\text{mb/GeV}^2$, with s and M^2 both measured in GeV^2. From this we conclude that we can identify an approximately energy independent contribution to the inclusive cross section which is due to the diffractive process with $d\sigma/dM^2)_{\text{inelastic diffractive}} = (2.9 \pm 0.1)/M^{3.7\pm0.1}$. The integral of this cross section has no logarithmic rise with s and is given over our s range by 1.8 mb. Because of the symmetry of the initial p-p state, the total inelastic differential cross section is twice the above value or, $\sigma_{\text{inelastic diffractive}} = 3.6 \pm 0.4$ mb for $262 \leq s \leq 741\ \text{GeV}^2$.

d) Note that our value for $\sigma_{\text{diffractive}}$ is much smaller than the currently accepted value of 6 to 9 mb. This is because the latter includes large contributions which are not diffractive (our value for this sum of diffractive and non-diffractive cross section is 6.6 mb). We have here for the first time unambiguously separated out the true diffractive

component of the inclusive cross section. Its magnitude of 3.6 mb is far from saturating the unitarity bound of $\sigma_{\text{inelas. diff.}} < 13$ mb.

e) Our data cannot be fit by a simple triple Regge[10] model formula and there appears to be no triple pomeron coupling.

f) We have no disagreement over measured quantities with other experiments performed in the past to determine inelastic diffraction. We disagree with the inferences drawn by other authors.

II. EXPERIMENTAL METHOD

A. Introduction

Very high energy inclusive scattering is much more precisely investigated by detecting the slow recoil proton rather than the fast forward particle because a) there is enormous amplification in the range of the scattering angle, b) the momentum transfer is directly the recoil momentum rather than a minute fraction of the forward particle's momentum. This method presents its own problems. Specifically, since most of the cross section is for $|t| < 0.2(\text{GeV}/c)^2$ and $t = -2mT$ where m is the proton mass and T its kinetic energy, one has to detect and measure protons with $T < 100$ MeV. While these energies are unusual in high energy physics, they are in fact very accurately measurable with proper techniques and precautions. For energies around 10 MeV, multiple scattering can become large and the proton range is only about

0.1 g/cm^2. Thus the target thickness must be kept well below such values, i.e. should be $\approx$ 0.01 g/cm^2. In addition, for the scattering angles of interest (45° to 90°), it is in practice difficult to cover large solid angles. Both these two constraints result in the necessity of very intense beams. In particular, to achieve reasonable data rates ($>$ 10^3 events/machine cycle), at least 10^{12} protons/sec on target are necessary. We ran a preliminary phase of this experiment in the external proton beam at Fermilab in the Neutrino Area.[11,15] Because of our interest in the energy dependence of the inclusive cross sections, the present experiment was performed at the ITA of Fermilab. Since the protons go around the Main Ring 50,000 times/sec, a typical accelerator intensity of 6 x 10^{12} protons per pulse corresponds to an on target intensity of 3 x 10^{17} protons/sec.

B. Target

This very high intensity is best matched by a target density of $\sim$ 10^{-7} g/cm^2. We used a target of about sixty 20μ $(CH_2)_n$ fibers and sixty 8μ carbon fibers mounted on a wheel rotating at 65 rps. These fibers hence had effective thicknesses of $\sim$ 1-2 x 10^{-5} g/cm^2. The appropriate interaction rate was achieved by inserting the fiber tips in the dense fringe of the beam from below (see Fig. 1). The main concern with the (CH_2) fibers was to prevent excess beam exposure which could produce heating and melting, resulting in enlarged tips of these fibers. In addition, the target had to be removed at injection so as not to produce large beam losses at low

beam energy, and then rapidly inserted and kept in the beam for 1 sec for each cycle. Finally, the beam shrinks in size during acceleration, has various slow oscillations, and sometimes sudden increases in vertical size during a cycle. For all three reasons the height of the target was continually adjusted by a closed loop servo which kept the interaction rate constant to within 20%. An optical synchronization signal told our data collection system which target was in the beam and all nuclear fragments production from each were constantly scaled. Target out versus target in rates were less than 0.1%, of which less than 1% would be candidates as acceptable events.

C. Proton Recoil Detectors

The proton recoils were detected by nine solid state detector telescopes. Eight were mounted on a movable carriage with a fixed angular separation of 2.406°. This carriage was mounted on a fixed arc centered around the target and by using a stepping motor and an absolute optical encoder, we could remotely position it in the range of 50° to 130° with a reproducibility of 0.01° and an accuracy of $\pm\ 0.05^{\circ}$. All these telescopes could be moved beyond 90°. One telescope was mounted at a fixed angle (83°) which is approximately the peak in the lab of p-p elastic cross sections. The fixed angle telescope monitored the (beam) x (hydrogen-in-target) luminosity by counting elastic recoils. The number of elastic protons per run in this fixed angle monitor provided relative normalization between runs.

A telescope consisted of 3 detectors, each a 1 cm^2 totally depleted silicon surface barrier solid state detector (D_0, D_1, D_2). Their respective thicknesses were 150 $\pm$ 15, 1000 $\pm$ 10, and 5000 $\pm$ 50 microns. The first detector was only used to define the acceptance of the telescope and not used in the energy determination. For this purpose, special detectors with charge collection electrodes deposited over only a small fraction of the active area were used (see Fig. 1). The electrode was deposited over a rectangular area 4 x 6 mm^2. Since the 4 x 6 mm^2 active area was sufficiently less than the size of the other two detectors, the edge effects for the thicker detectors which would impair resolution were eliminated. The edge effects of D_0 reflect themselves only in a 10% momentum dependence in the solid angle acceptance which can easily be calibrated. The detectors rotated on an arc of radius 92 centimeters centered at the target subtending a solid angle of 2 x 10^{-6} sterad per telescope with an acceptance in θ of $\pm$ 0.125^{o}. Calibration of the relative solid angle of each telescope was performed by positioning each telescope at an identical angular position and counting the number of elastic proton recoils per monitor proton. This information gives the relative normalization between telescopes. The whole detector-carriage system was enclosed in a vacuum chamber which was directly connected to the Main Ring. A 0.2 mil aluminized mylar window reduced electromagnetic beam induced noise.

Since carbon nuclei were present in our targets, copious nuclear fragment production (d,t,He^3,He^4...) was observed,[12] a fortuitous fact which rendered our application of the standard CH_2-C method elegantly accurate (see Sec. III.A). The telescopes therefore performed the following functions: a) produced a trigger, b) identified particle type, c) measured T, d) measured θ. The telescopes are sketched in Fig. 1. The trigger was provided by a coincidence between D_0 and D_1. The particle identification was provided by detectors D_1 and D_2 for particles stopping in D_2. The identification was by means of the well known method of using the correlation between the energy deposited signals E_1 and E_2, measured in the form of charge produced in the totally depleted Si crystal by the ionizing particle. The correlation for stopping p, d, and t is given by the upper branches of the respective curves in Figs. 2a and 2b. T is obtained as the sum of E_1 and E_2.

We note here that if we were to limit ourselves to protons which stop in D_2, we could only measure proton energies up to 35 MeV in our setup. Since the cost of the amount of Si necessary to stop 100 MeV or more protons is prohibitive, we have extended the method to higher energy protons which fully cross D_2.[13] These latter protons have higher energy than the stopping protons, hence ionize less, causing the correlation curve to fold back as shown in Figs. 2a and 2b. Assuming the detected particle to be a proton, a good T measurement can be obtained from the measured E_2 value. The $T(E_2)$ relation can be derived from a knowledge of the range energy relation for protons in Si and of the exact thickness of the detectors

trivially to 1%. We preferred instead to obtain the $T(E_2)$ relation for each telescope empirically by placing it at known angles and observing the position of the elastic peak whose recoil energy was calculated from kinematics. The relative $T(E_2)$ relations between these almost identical telescopes were determined to 1/4%. The E_1 vs. E_2 plots were displayed online during data taking as they are extremely sensitive monitors of running conditions. Any sudden change in the whole chain of data collection apparatus (including for example accelerator conditions) visibly alters the width, position, density of points both on the correlations curves and over the whole E_1 E_2 domain. In particular, this also turned out to be a rather sensitive method of monitoring background since any source not at the position of the target caused events to cross the telescope at rather large angles, destroying the range-energy correlation. Since most of these events are high energy events, they tended to fill the minimum ionizing corner of the plot. However, the correlation curve for pions is located near the minimum ionizing point (see Fig. 2a). Since pions are not copiously produced at large angles in the lab, it is difficult to observe this correlation curve if even the slightest amount of background were present. All of our data were taken under conditions where the background was low enough to observe the pion curve (see Fig. 2b). Our kinetic energy range was from 12 to 120 MeV, with about 200 KeV (FWHM) energy resolution at low T and increasing to about 5 MeV at the highest T.

D. Electronics

All the electronics used were designed and constructed for the present experiment.[14] Solid state detectors require charge sensitive amplifiers with sensitivity of $\sim$ 1 V/pC, noise $\sim$ of 5×10^{-3} pC, to fully use the Si detector energy resolution. To obtain reasonable resolving time, the rise time of the output signal from the charge sensitive amplifiers (preamps) must be $\leqslant$ 50 ns. We have designed preamps with these characteristics. Their typical rise time is $\sim$ 20 ns into a 50 Ω load. These preamps moreover operate in vacuum which added a constraint in design due to power dissipation considerations. The preamp itself was placed within 2 inches of the detector to minimize noise and rise time. The detector-pre-amp assembly was kept at 70°F $\pm$ 5°F by a heat exchanger; at such temperature and constancy, any gain change due to temperature variations was < 1/4%.

Since the experiment itself was underground in the Main Ring tunnel and approximately 150 ft of cable was necessary to bring a signal to the electronics trailer, the preamp signals were fed to delay line clipping linear amplifiers prior to their transmission through the long cables. The linear amplifiers have a gain of 10, rise time of $\sim$ 50 ns and clipping time of $\sim$ 1 μs. The combination of charge preamp and differentiating amplifier shows no loss of energy resolution for pileup to a DC output from the preamps corresponding to 50 times the magnitude of single particle signals. The analog signals were fed to discriminators and to a second delay line amplifier followed by a track and hold amplifier. One such channel was used for each detector.

A master trigger signal was produced upstairs as the "or" of the D_0 D_1 coincidence from all the telescopes. A flag was set also for each telescope giving a coincidence within 50 ns of the master trigger. See Fig. 3. The master trigger switched after appropriate delay all track and hold amplifiers to their hold mode. A small amount of TTL logic was used to scan, upon receipt of a master trigger, all the flags. When an active telescope was found, the corresponding energy signals were switched through a set of SOS MOS switches from the track and hold amplifiers to two 12 bit successive approximation analog to digital converters whose outputs were the E_1 and E_2 values in digital form, see Fig. 4. An event was thus defined by: a) the two 12 bit E_1 and E_2 numbers (which will yield T and particle type), b) a 3 bit number identifying at which time of the acceleration cycle the event had occurred (which will yield E_{beam}, hence $s \approx 2m_p(E_{beam} + m_p)$), c) a 4 bit number identifying which telescope recorded the event (which will yield θ), d) a bit identifying whether the $(CH_2)_n$ or the C target was in the beam during the event's occurrence.

Whenever a single detector triggered its discriminator, an updating 2μs deadtime was generated. The "or" of two deadtime signals from the two discriminators of each telescope was used to gate a scaler, for each telescope and energy gate, which counts a clock whose frequency was proportional to the instantaneous beam-on-target intensity. This gated count

divided by the total clock count was a measure of the deadtime. The deadtime scalers counts were recorded for each carriage position. Deadtimes were measured only for the $(CH_2)_n$ targets since their deadtimes were used to combine data from different telescopes after the free hydrogen distributions had been obtained. Deadtimes were typically of the order of 1 to 7% varying monotonically with angle and they were measured to 1.5%.

E. Real Time Analysis

During setup, tuning and data taking in this experiment, well above 10^9 events as described above were taken. A minimum format for the above data would consist of two 16 bit words per event. Because of possible multiple events, 4 words were used. In the standard way of dealing with this information, one might fill a portion of the memory of a computer and write the memory content on tape whenever the memory was full. Three disadvantages were encountered with this method. First, the event rate was limited to the capacity of the buffer memory available. Second, a tape could only record a theoretical limit of 2.88×10^6 events. Third, the collected data must first be reduced to yield the information of particle type and T etc., then a map of $d\sigma/dTd\Omega$ had to be produced. If this last step were performed on a reasonably large (i.e., 370/155) computer, we found that it required $\sim$ 1 ms of CPU time to fully dispose of an event. A small portion of our data, i.e. one tape or 0.3% of the data, would thus require approximately 1 hour of CPU time or typically a couple of days of calendar time to be reduced to a histogram of a physical cross section.

In a general purpose computer, most of the time is spent in fetching instructions from core, obtaining and returning data to core, and in preparing input and output references. With the advances in solid state technology in the late 1960's, it became clear to us that it should be possible to perform the complete event reduction with a specially built hardwired computer in less than 1 μs, a time scale small compared to the analog and digital operations described previously. The components needed for building such a special purpose computer (2000 8-bit words of memory with 45 ns read time, 16 bit adders with ≈ 40 ns propagation time, 4 x 4 bit multipliers with 80 ns execution time, various multiplexing, demultiplexing and magnitude comparison IC's) were relatively inexpensive and available, such that an efficient program could be constructed with hardware with a gain in speed of a factor of a thousand and for a cost equivalent to executing the program 10^6-10^7 times on a general purpose computer. This fact was borne out during the analysis of our two experiments.[13]

In detail, the special purpose calculator (called here the Event Analyzer or E-A) built for this experiment operates as follows: For every event E_1, E_2, telescope number, energy gate are input into the E-A. Only E_1 and E_2 are actively used. The 12 bit E_2 word is divided into the 8 most significant bits called from now on, E_2, and the 4 least significant bits, called ΔE_2. E_2 addresses one of the 256 locations of 10

separate sets of memory of the appropriate number of bits. Figure 5 shows these memories and what is stored in each. For each value of E_2, the memory contains tables of the corresponding values of E_1 for protons, deuterons and tritons as well as for protons crossing D_2. E_1 values are stored as 8 bit words. An acceptance width for each correlation is also stored. The main operation performed by the E-A is the comparison of the measured E_1 value (truncated to 8 bits) with the stored E_1 value to identify particle type. For stopping protons, T is calculated by direct addition of the full precision E_1 and E_2 values. A different method is used to calculate T for particles crossing D_2. The function $T(E_2)$ and its derivative are stored in memory also. The first two terms in the Taylor expansion of T are calculated as shown in Fig. 5. If a particle is recognized as a non-stopping proton, it is this last value of T which is chosen. The four cases, crossing proton (proton down), stopping proton (proton up), deuteron and triton are checked sequentially in their most likely occurrence order. Figure 5 shows the memory outputs for the crossing proton case. Note how four words are simultaneously output. Each path is linear and noniterative. The total propagation time for the crossing proton case is 156 ns, 95 ns are necessary for each new case, giving an average analysis time of $\sim$ 200 ns. The E-A end product is a T value which is packed together

with telescope number, energy gate number, particle type and target type to form a single 16 bit word. Finally, this word is used to address a location in a PDP-11 memory into which 1 is added. Since the addition was performed by the PDP-11, which used a stored program, this last step took some 10 μs!

The result of the above described operations is a three-dimensional map in core of $d^2N(s)/dTd\Omega$. If 65,000 words of 16 bits each are available for storage, events can be accumulated until any one bin in the map should reach a count of 65,535. This would happen in our experiment every 10^8 events. At this point, the whole memory would have to be copied onto tape requiring ~ 160 inches of tape. In our case, since we had only 16,000 words of PDP-11 memory available, we addressed half-words to increment their contents and were therefore limited to 255 counts per bin. Deuterons and tritons were recorded as total count (without T) and required an extra 1000 words of memory. The cross section was therefore written on tape for every 300,000 events using 40 in. of tape. Thus 10^9 events were contained in about four tapes as compared to 500 tapes. In fact, the histograms were dumped onto tape every 10 to 15 minutes (about 1/2 million triggers) to minimize possible loss of data due to tape error or other possible failures. Note that 50% of the triggers had already been rejected. Most of these came from minimum ionizing particles whose energies were greater than 140 MeV.

Because of the Event Analyzer, we were able to process approximately 1 billion triggers in a short enough time to allow us to retake any data which were suspected of having background, thus eliminating the necessity of any correction for it. The background level in this experiment was reduced to 1/10,000 of the accepted events and this minute level was isotropic.

III. FINAL DATA REDUCTION

A. Free H_2 Cross Section

From the three-dimensional maps of $dN(s)/dTd\Omega$ described above, the cross section in free H_2 can be obtained by subtracting run by run and telescope by telescope the carbon data with appropriate normalization from the poly data. The proper normalization was obtained by counting deuterons and tritons produced in carbon and in poly in each run, simultaneously with the counting of proton recoils, in the identical telescope. Hence the ratio of these nuclear fragments from the two targets gave directly the correct ratio (effective beam intensity x carbon in target) with no correction necessary for beam duty dycle and telescope deadtime.[12] Thus, despite the fact that free proton interactions were approximately 10% of the total beam poly interaction, the subtraction was performed to high precision ($\approx$ 2 parts in 10^3). The measured individual deadtimes were applied to the subtracted free H_2 distribution when combining different runs ($\approx$ 3.5% on the average).

The free H_2 $dN(s)/dTd\Omega$ was transformed bin by bin to $dN(s)/dtdM^2$ by computing the appropriate jacobian. These distributions, when normalized appropriately by multiplying with a normalizing constant (see next section), yielded $d\sigma(s)/dtdM^2$, of which Fig. 6 is a typical plot: $d^2\sigma/dtdM^2$ vs. M^2 for an s of 565 GeV^2 and $0.023 < |t| < 0.080$. It is plotted on a log-log scale to demonstrate our extremely good mass squared resolution and to show our total M^2 range. M^2 is expressed in terms of (T,θ) by $M^2 = m_p^2 + 2p_{beam}p_{recoil} \cos\theta - 2(E_{beam} + m_p)T$.

Our mass resolution is dominated by the angular resolution at low T ($\pm$ 0.125°) yielding 1 GeV^2 (FWHM) at 300 GeV/c incident beam momentum. At high T, it is dominated by the kinetic energy resolution and becomes 3 GeV^2 (FWHM).

B. Elastic and Inelastic Events Separation

These cross sections contain both elastic and inelastic contributions (as seen in Fig. 6). The elastic and inelastic contributions to the data were trivially separable at low beam energy ($E \sim 50$ GeV) as the elastic peak was completely separated from the continuum. At such energies, one notes that the peak indeed has the expected shape of a gaussian folded over the T interval equivalent to the angular acceptance of the detectors (see Fig. 7). Such a symmetric gaussian shape persists even as the mass resolution broadens linearly with the increase in beam energy (as in all recoil proton experiments) and the elastic peak merges with the inelastic

continuum (see Fig. 6). In all cases, the elastic peak falls *for* $M^2 < m_p^2$ *by more than three orders of magnitude and is* well below the inelastic signal.

While we can separate elastic and inelastic contributions in the $dN(s)/dtdM^2$ histograms, we prefer to do the separation directly from the $dN(s)/dTd\Omega$ mappings because our resolution function in T is independent of beam energy and angle and its parameters can be calibrated at beam energies where the èlastic events are separated from the inelastic continuum (from E_{beam} = 8 GeV to about 100 GeV). From the knowledge of the T resolution function, the central value of the elastic peak (as measured at low beam energies) and the fact that kinematically the inelastic events must have less energy than elastic events at the same angle, the elastic and inelastic contributions to each measured spectrum are unambiguously separated. This separation is very good over our whole T range because of our good resolution (see Sec. II.C) and the absence of background. Typical results of such separation are shown in Figs. 8a,b,c up to the highest T. The dashed lines are the fitted curves to the data. The form used to fit was the sum of a δ function at the elastic position and an arbitrary polynomial which is constrained to vanish above the kinematically allowed maximum T value, folded with our experimentally determined resolution function.

We note that the functional form also includes the multiple scattering effects from our thin targets which are

negligible except at extremely low T ($\approx$ 15 MeV). The net effect of multiple scattering at T $\approx$ 15 MeV is approximately 100 KeV shift of the center and a 1% asymmetric broadening of the peak, almost invisible in Fig. 8a. At the high end of the T range (T $\sim$ 100 MeV), where the elastic contribution has fallen greatly and has become comparable to the inelastic contribution, there is an apparent 1% shift in the elastic peak position due to the two contributions (see Fig. 8c). The aforementioned knowledge of the peak positions at low beam energies, where the inelastic is completely separated from the elastic, allows us to uniquely separate the elastic from inelastic data. Hence throughout our and T range, we have a complete determination of the relative elastic and inelastic contributions in the dN/dT plot in the elastic region and the elastic contributions (solid lines in said figures) were removed to yield the inelastic contribution. Incidentally, varying the parameters of the resolution function, including width, by a factor of 2 or so, does not affect the inelastic spectrum above mass squared of 2 GeV^2 because our mass resolution is so narrow that only the tail of the inelastic overlap the elastic region.

C. T Dependence of Solid $\measuredangle$ Acceptance

In any spectrometer, the momentum scale, as well as the system's acceptance as a function of momentum, is obtained by calibration through the incidence of monoenergetic

beams upon the system. In our case, the elastic proton recoils provide us with monoenergetic beams throughout our T range. As has been stated in Sec. II.C, they allow us to check our $T(E_2)$ function, calibrate the relative $T(E_2)$ functions of each telescope and the relative acceptances of the telescopes as a function of T, which were identical to within 2%. Finally, they allow us to calibrate our acceptance as a function of T if dN/dT vs. T is known at any s. Our acceptance is 95%, uniform across our T range. The small nonuniformity exists because detector D_0 has a small effective increase in area for low T ($\approx$ 15-25 MeV) events. The size of the effect was measured in the following manner: Plots of $d\sigma_{el}/dt$ vs. t were first obtained without assuming any T dependence in the solid angle acceptance (for a typical plot, see Fig. 9, elastics from a subset of data at 300 GeV/c). The t range was split into two pieces, namely from $0.032 < |t| < 0.113$ and from $0.113 < |t| < 0.234$. The elastic data were then fit to the form Ae^{bt} over each range but requiring that they have the same value at $t = -0.113$ (T = 60 MeV, close to where we performed the absolute normalization). The slopes so obtained agreed within 10% with those obtained by experiments designed to measure elastic scattering to high precision.[16] Our slope values tended to be high by 1.5 GeV^{-2} in the low t region and were consistent in the high t region. This was seen, independent of telescope, runs and beam energy,

confirming its systematic nature in favoring trigger acceptance of low T events. Therefore, assuming at 200 GeV the correctness of the Fermilab measurement,[16] we have measured our acceptance as a function of T, which can then be applied to all our data at different s values since as stated our resolution function in T and fixed θ is independent of beam energy. When such is done, we note moreover that the change in slope between the two regions $\Delta b = b_{low\ t} - b_{high\ t}$ is about 1.1 GeV^{-2} and is present over the whole range of our s measurement (see Fig. 10). The magnitude of this effect is in agreement with other measurements at Fermilab and ISR[17] performed at different s values from our experiment. The present data are not accurate enough to differentiate between a "break" and a continuous change in slope of the elastic.

It is noteworthy that one need not even correct this small (5%) lack of uniformity in acceptance over our T range, when considering $d\sigma/dM^2$ (integrated over T) since our range covers 70% of the cross section and the fraction of coverage is identical as long as the slope lies between 6 and 19, see Fig. 14.

D. Conversion to Absolute Units

Since the actual beam intensity on target in this experiment was not measured, the cross sections $d^2N(s)/dtdM^2$ were obtained in arbitrary units. The elastic contributions were used to get the normalization constant which transforms from $d^2N/dtdM^2$ to $d^2\sigma/dtdM^2$ for each set of data, in particular

we used our measured elastic cross section at $t = -0.094$ equating it to $d\sigma_{el}/dt$ at the same t. (26.65 mb/GeV^2). The absolute normalization was performed at this particular t because over our s range of 160 GeV^2 to 741 GeV^2, $d\sigma_{el}/dt$ at $t = -0.94$ was independent of s to 1%, see Appendix A.

E. Corrections

The corrections necessary in this experiment to be applied to the raw subtracted H_2 spectra are minor ($\approx$ 2%). Were they not applied at all, the characterisitc of the spectra would not have altered.

There was an unplanned complication at very low T, i.e. 2% of our T range, ($T \leqslant 15$ MeV) in the otherwise ideal bin by bin $(CH_2)_n$-C subtraction method used to obtain the free proton distributions, namely that the two targets were of different thicknesses, especially since the poly fibers tended to melt in the beam and increase their girth. We recall that our T scale which assigned T values to each bin was determined by the measurement of the elastic proton scattering (knowing the scattering angle), hence correctly represented the energy of the recoil proton from an interaction within the poly fiber, independent of energy loss in escaping the poly target. Therefore, a correction factor (1% at 15 MeV, negligible thereafter) dependent on the difference in thickness between the two targets was applied both bin by bin to the carbon proton distribution and to the deuteron

normalization factor before the subtraction was performed. The average thickness of the poly target, weighted by our live time, was calculated using data taken at angles and T values which were kinematically forbidden to free protons (negative mass squared region), but not to carbon protons with their Fermi momentum, together with the deuteron counts and knowledge of proton to deuteron cross sections as a function of T measured from our previous experiment.[11,15] The target thickness information was thus used in the calculations of the 100 KeV shift and 1% asymmetric broadening of elastic peaks due to multiple scattering at low T ($T \approx 15$ MeV), see Sec. III.B. The subsequent modification in T scale and in decrease of events in the Poly distribution at low T due to this effect was small ($< 2\%$) and was corrected for.

Nuclear interactions in the detectors (which could cause mismeasurement of the total energy) were negligible, giving effects of $< 1\%$, and were not corrected for.

IV . RESULTS

A. General Features

This experiment resulted in a 4000 point three dimensional mapping of the doubly differential inelastic cross section $d^2\sigma/dtdM^2$ as a function of s. Innumerous two dimensional projections were examined during the analysis to decide the best method for synthesizing and extracting physics results from the data. For example, Fig. 11 shows $d^2\sigma/dtdM^2$ for $t = -0.075$ vs. M^2 at three different s values in the low mass region. The dominant feature clearly is a large peak at low M^2, independent of s, falling sharply as M^2 increases (much sharper than $1/M^2$). The area of this peak is largely independent of s, the height variations seen in the figure just reflect our broadening mass resolution with increasing s. Note that the use of the Feynman variable x ($\sim 1-M^2/s$) as the independent variable in this region would have introduced an apparent energy dependence to this energy independent (diffractive) peak.

Figure 12 shows $d^2\sigma/dtdM^2$ integrated over our t range (for statistics) for three values of s, emphasizing the high mass region. The cross sections at large M^2 have levelled out. Also the three sets of data are vertically displaced by a constant amount for all M^2 values. The value at which the cross section appears to

level out falls as 1/s. In fact, the heights marked on the graph with a solid line next to the large M^2 cross sections are values of 11/s, evaluated at each appropriate s. These constant separations moreover extend down to very low masses, within statistics probably down to threshold (in this figure over the whole mass range plotted).

Figure 13 shows typical t dependence observed in our data for fixed s(565). To reduce systematic fluctuations, the data have been averaged over five large mass intervals and typical errors are shown in the $20 < M^2 < 50$ GeV^2 bin. Noteworthy features of the inelastic data t dependence are that for all M^2 regions, the slope resulting from fits to the form Ae^{bt} are greater than 6 $(\text{GeV})^{-2}$. Limited statistics in this experiment do not allow a complete study of M^2 vs. t and s. Of importance however is the fact that this experiment observes about 65% of the total inelastic cross section (per given s and M^2) independent of b as long as the inelastic cross section can reasonably be described by a simple exponential t dependence whose slope lies between 6 and 19 (see Fig. 14).

B. Integrated Cross Sections

Aided by the insights obtained from the examination of the aforementioned two dimensional projections of the data, we decided that cross sections integrated over our range in t and from threshold to various fractions of s: a) gave a direct measurement of whether the "diffractive" region was responsible for the increase in the total cross

section as a function of s, b) greatly reduced (by a factor of ~ 100) the number of data points, c) eliminated the need of detailed knowledge of mass resolution and t dependence as a function of M^2 and still allowed the determination of the mass spectrum as a function of s.

The data presented in Table 1 were obtained by first summing $d^2\sigma/dtdM^2$ for fixed mass over ten t intervals, from t = -0.024 to t = -0.234, and then summing over mass from threshold to $\eta s + m_p^2$ for five different values of η.

Table 1

s GeV^2 / fraction η	262	309	366	565	741
0.10	2.00 ±0.028	2.06 ±0.028	2.03 ±0.028	2.02 ±0.028	2.16 ±0.030
0.06	1.57 ±0.026	1.60 ±0.026	1.59 ±0.026	1.65 ±0.026	1.72 ±0.027
0.04	1.31 ±0.024	1.33 ±0.024	1.33 ±0.024	1.42 ±0.024	1.49 ±0.024
0.02	0.93 ±0.022	0.95 ±0.022	0.96 ±0.022	1.11 ±0.022	1.18 ±0.022
0.01	0.60 ±0.020	0.62 ±0.020	0.64 ±0.020	0.82 ±0.020	0.90 ±0.020

$$\sigma = \int_{0.024}^{0.234} dt \int_{th}^{\eta s+m_p^2} dM^2 \left(\frac{d^2\sigma}{dtdM^2}\right)$$

These are directly measured quantities which demonstrate that, as long as the low mass peak is included in the cross section measurement, the total cross section in the "diffractive region", i.e. from threshold to any fraction

$(0.05 < \eta < 0.1)$ of s, is essentially independent of s. These cross sections are consistent with an increase with s of the same fractional amount as the total cross section ($\sim$ 5%), and clearly are in contradiction with the postulate that the total rise in cross section of 0.7 to 0.9 millibarns occurs in this low mass region. For comparison with other measurements, we extrapolated our measurements to include the remaining t domain by multiplying our results by 1/0.65. The results are plotted in Fig. 15 for five different values of η and seven values of s.

The cross section obtained by integrating the data over t and extended using (1/0.65) has now the following uncertainty because of the possibility of a flattening of the inelastic slope at high t;[18] namely this introduces an asymmetric error (since it is probably not steeper at large t) of +10%, -2%. This is essentially a scale factor since it is independent of s and M^2.

C. Mass Dependence

The integrated cross section points on Fig. 15 were used to perform a fit to the form $d\sigma/dM^2 = A/s + B/M^{\alpha}$, yielding $A = 15.0 \pm 0.5$, $B = 2.9 \pm 0.1$, and $\alpha = 3.7 \pm 0.1$ with a $\chi^2 = 33$ for 22 degrees of freedom. The low energy ($s = 114$, 160 GeV^2) points were not used in the fit. However, looking at the points and at the solid lines in Fig. 15a, which are the above mentioned fit, one notes that our fitted form is valid down to $s \sim 100$ GeV^2. Figure 16 shows the fitted curve $d\sigma/dM^2 = 15/s + 2.9/M^{3.7}$ superimposed on a typical set of data at $s = 366$ GeV^2. We note the excellent agreement and the validity of the method of using the integrated cross sections to obtain the mass spectrum. An actual fit to only the data in Fig. 16 gives slight different values of A and B which are consistent with A = 15 and B = 2.9.

The degree to which our data rejects other values of α can be seen by the resulting increase in χ^2 values when we impose specific values of α during the fit. They are: $\alpha = 4$, $\chi^2 = 42$; $\alpha = 3$, $\chi^2 = 105$; $\alpha = 2$, $\chi^2 = 1017$. Hence it can be summarized that our data's best fit is $\alpha = 3.7 \pm 0.1$, it could probably accept $\alpha = 4$, it definitely is inconsistent with $\alpha = 3$. It categorically rejects $\alpha = 2$ (see Fig. 15b) which is the mass spectrum dependence which would trivially have predicted that the low mass region was responsible for the rise in the total cross section with s

$$\left(\int_{th}^{\eta s} \left(\frac{A}{M^2}\right) dM^2 = A \times \ln(s) + \text{constant}\right).$$

D. Magnitude of "Diffractive" Cross Section

According to Good and Walker, inelastic diffraction is independent of s whenever the coherence condition $\Delta\lambda < r$ is satisfied, i.e. for states of mass M such that $M^2 \leqslant s \times (m_\pi/m_p)$. Hence it is of interest to study the magnitude of such an s independent term in the mass spectrum, as it could be a dominant process at high s where large M^2 values can be coherently produced (50-100 GeV^2 in the present experiment). We identify the B/M^α term of our fit (which is s independent) as the "diffractive" cross section in the Good and Walker sense. Hence the total "diffractive" cross section, taking into account the symmetry of the initial pp state, is $2 \times \int_{th}^{\infty} \left(\frac{2.9}{M^{3.7}}\right) = 3.6 \pm 0.4$ millibarns. This magnitude is small compared to the total inelastic cross section and is about half of the elastic cross section. Also, the contribution

of this diffractive term essentially vanishes at $M^2 \sim 20\ GeV^2$, significantly before the maximum mass values allowed by the coherence condition.

E. Comparison with Other Experiments

The major experimental effort to study pp inelastic scattering at small momentum transfer at ISR was made by the CHLM group.[18] There is some overlap in the s, t and mass regions studied by CHLM ($M^2 < 50\ GeV^2$, $0.15 < |t| < 1.75$, at $s = 549\ GeV^2$ and $725\ GeV^2$) and by this experiment. A few years ago, the Rutgers-Imperial College (R-I) collaboration performed an experiment[19] in our s range at Fermilab for a small fraction of the cross section, $0.14 < |t| < 0.38$ and $0.07s < M^2 < 0.2s$. Recently the FSASG at Fermilab published some inelastic results at $s = 296\ GeV^2$, $3 < M^2 < 9\ GeV^2$ and $0.1 < |t| < 0.625$.[20] In the low mass, low t region we overlap with two Soviet-US efforts,[21] $0.01 < |t| < 0.05$, $1.3 < M^2 < 3.7$, $330 < s < 752$ with $p+p \rightarrow p+X$ and $0.03 < |t| < 0.12$, $M^2 < 35$ from $p+d \rightarrow d+X$ and extracting the nucleon-nucleon cross sections by factorization. Many bubble chamber experiments studied the reaction $p+p \rightarrow p+X$ and collectively they cover a vast s,t and M^2 range but are limited by statistics.[22] Finally, there was our previous experiment[11,15] at $s = 569\ GeV^2$, covering a similar t range, with M^2 extending to 0.17s, and there is our current experiment[23] at the ITA using a hydrogen jet target, where the t range

is extended to 0.5 and s range is extended to s = 939. The present experiment is in agreement with both our previous experiment and with the preliminary results of our current experiment.

For comparison with other experiments, we note that wherever data overlap, we and the other experiments agree to within 20%. For example, all the experiments find the inelastic slope b (of Ae^{bt}) to be ~ 6 for $5 < M^2 \leq 50$ GeV^2. In Fig. 17 we see the ISR and R-I points superimposed over ours, showing agreement in both magnitude and t dependence of the differential cross section. In Fig. 12, the value of $d\sigma/dM^2$ (the dashed line) from R-I is shown next to our data. They indicate that while there may be a 15% relative normalization difference between the two experiments, the s dependence of the high mass data is similar. In Fig. 5, four points from the Soviet-US collaboration are plotted (adjusting for the fact that their measurements were made at s = 516 instead of 565, and using our s dependence), again exhibiting that there is no significant divergence of experimental values. Inspection (see Appendix B) of our cross section values in the s, t and M^2 ranges which overlap those of FSASG clearly indicate agreement. Finally, we note that ISR finds for $2 \times \int_{th}^{0.1s} (\frac{d\sigma}{dM^2}) dM^2$ to be 7.61 ± 0.23 at s = 549 and to be 7.24 ± 0.53 at s = 725, having extrapolated to include the unmeasured $|t| < 0.15$ region. From Fig.15a one sees that our corresponding two values are 6.44 ± 0.38 at s = 549 and 6.53 ± 0.34 at s = 725.

We recall that these integrals were obtained by extrapolating over the remaining t domain unmeasured by us by assuming a simple exponential. However, if the inelastic slope indeed flattens out at high t as measured at ISR (b goes from 6 to 4), then our values should be revised upwards by $\sim$ 10%. Hence the comparison is between 7.61 and 7.08 at s = 549, and between 7.24 and 7.15 at s = 725, clearly good agreement.

The CHLM experiment, however, reports a spectrum like $1/M^2$. Since we have shown that both our integrated and high mass cross sections agree well with their results, we suggest that the different shape observed at ISR is due to the wider M^2 resolution ($\sim$ 10 GeV^2) of their experiment. FSASG and the Soviet-US collaborations also quote a $1/M^2$ mass spectrum, except the latter modified by a partial s dependence. In this case we believe that it is the limited range of their M^2 measurement which led to such a formulation. This is best demonstrated in Fig. 18 where $M^2 d\sigma/dM^2$ is shown for two s values together with the Soviet-US formula prediction. It is apparent that $M^2 d\sigma/dM^2$ is flat for only a very narrow region of M^2 and that region is different for different s values, hence $1/M^2$ cannot be the correct mass spectrum dependence for the s independent part of the cross section.

F. Comparison with Theoretical Conjectures

While our fitted spectrum is of the form $d\sigma/dM^2 = 15/s + 2.9/M^{3.7}$, dimensional arguments suggest for the energy independent cross section $d\sigma/dM^2$ = constant/M^4. Similarly,

for the scaling term, the only scale is fixed by σ_{tot}, resulting in $d\sigma/dM^2 = g(M^2/s) \times (\sigma_{tot}/s)$, where $g(M^2/s)$ appears to be remarkably constant up to $M^2/s \sim 0.1$. It is therefore logical that the inelastic spectrum should be of the form $d\sigma/dM^2 = A/s + B/M^4$. If we constrain $\alpha = 4$, we obtain $A = 16.0 \pm 0.5$ and $B = 3.5 \pm 0.1$, with $\chi^2 = 42$ for 23 degrees of freedom.

We believe that we have truly separated the "diffractive" cross section, i.e. the energy independent part of the cross section, from the rest of the inelastic cross section, and its value is 3.6 ± 0.4 millibarns. We note that this value does not contradict the Pumplin bound $\sigma_{diff} < 1/2\ \sigma_{tot} - \sigma_{el} \simeq$ 13 mb, or the ratio $R(s) = (\sigma_{el} + \sigma_{diff})/\sigma_{tot}$, determined by us to be ~ 0.25, half of the saturation value of 0.5.

For completeness, we have also fit our results to the Triple Regge[10] formula for the inclusive inelastic cross section:

$$\frac{d^2\sigma}{dtdM^2} = \frac{1}{s^2} \times [G_{PPP}(t) \left(\frac{s}{M^2}\right)^{2\alpha_P(t)} (M^2)^{\alpha_P(0)} + G_{PPR}(t) \times \left(\frac{s}{M^2}\right)^{2\alpha_P(t)} (M^2)^{\alpha_R(0)} + G_{RRP}(t) \left(\frac{s}{M^2}\right)^{2\alpha_R(t)} (M^2)^{\alpha_P(0)}]$$

using $\alpha_P(t) = 1.0 + 0.28t$ (obtained from Ref. 24) and $\alpha_R(t) = 0.5 + t$ (obtained from Ref. 10). We obtained $G_{PPP}(0.1) = -0.62 \pm 0.1$, $G_{PPR}(0.1) = 6.6 \pm 0.2$, and $G_{RRP}(0.1) = 48 \pm 2$ with $\chi^2 = 71$ for 22 degrees of freedom. Aside from the unacceptable χ^2 value showing the above is

a poor fit, a negative G_{PPP} term means we do not have a physical solution. Therefore we conclude that the Triple Pomeron contribution in our data is negligible and that the Triple Regge formalism does not describe our data. Finally if one were to insist that by looking at our data (for example, Fig. 18) that some Triple Pomeron contribution exists because there is some apparently flat region ($M^2 \times 1/M^2 = k$) for a narrow region of M^2, one would be hard put to explain why the position of this region as well as its value should be s dependent, since the Triple Pomeron ($1/M^2$) term should be independent of s.

We wish to thank the staff of the Fermilab Accelerator Division, especially the Internal Target Area operating crew and Dr. Drasko Jovanovic; the Nevis machine shop where most of the mechanical construction was performed and A. Teho for the design work; the Nevis electronics shop and Tom Tarantowitz of Stony Brook for construction of some of the electronics; W. Sippach of Nevis Lab for help with developing the Event Analyzer.

APPENDIX A

Absolute Normalization

Elastic peaks as a function of T were fit to obtain the number of events per millibarn of elastic cross section. This was the number of events per millibarn used to normalize the inelastic data to obtain the cross section. We have used the value 50.0 millibarns per GeV for $d\sigma_{el}/dT$ at T = 50 MeV for all s. If a small s dependence of $d\sigma_{el}/dT$ at T = 50 MeV were observed, our data at any energy could be renormalized by multiplying all the data points by the appropriate s dependent constant.

The absolute normalization was done at T = 50 MeV because $d\sigma_{el}/dT$ at t = -0.094 is relatively independent of s. The following values as a function of s were obtained[24] from $b(s) = 8.23 + 2 \times 0.278 \times \ln(s)$ and $\sigma_{tot}(s) = 38.2 + 0.49 \times \ln^2(s/122)$.

s	$d\sigma_{el}/dT$ at T = 50 MeV
114	51.0
160	50.2
262	49.6
309	49.5
366	49.5
565	49.8
741	50.2
Average	50.0

APPENDIX B

Differential Cross Section Tables

The tables consist of five sets (one for each average s value) of $d^2\sigma/dtdM^2$. Each table has four bins in t, the average value of which heads each column, and has up to sixty bins in mass squared, the average value of which labels each row. The four t bins are from $13 \leq T \leq 25$ MeV, $25 \leq T \leq 55$ MeV, $55 \leq T \leq 85$ MeV and $85 \leq T \leq 125$ MeV, respectively. Each bin consists of two numbers, the final value of the cross section and its error. A zero error means that no determination of the cross section has been made for that bin. The errors are statistical and they usually dominate over any systematic errors in subtraction or normalization. The only exception being the data at the lowest t column, near the N*(1400) peak where the statistical error is small ($\simeq$ 1%) but the error (which is an estimate of the uncertainty in the calculation) due to uncertainty in size and shape of the target thickness is about 10%. For all other t columns, that uncertainty is negligible (< 1%). Finally, if the t dependence at low t as measured by the quoted Fermilab experiment[16] were incorrect, our data should then be corrected by some t dependent "solid angle" effect, and the correction would be independent of s and M^2.

References

1 M.L. Good, W.D. Walker, Phys. Rev. 120, 1857 (1960).

2 C.E. DeTar et al, Phys. Rev. Lett. 26, 675 (1971); D. Silvermann, C-I. Tan, Nuovo Cimento 2A, 489 (1971) and Phys. Rev. D3, 991 (1971). N.F. Bali et al, Phys. Rev. D3, 1167 (1971); G. Chew, A. Pignotti, NAL Summer Study (1968).

3 U. Amaldi et al, Phys. Lett. 44B, 112 (1973); S.R. Amendolia et al, Phys. Lett. 44B, 119 (1973).

4 A.S. Carrol et al, Phys. Rev. Lett. 33, 928 (1974).

5 A. Capella et al, Phys. Rev. Lett. 31, 497 (1973).

6 F.K. Loebinger, in Proceedings of the XVIIth International Conference on High Energy Physics, London, England (1974), I-71, edited by J.R. Smith (Rutherford High Energy Laboratory, Didcot, Berkshire, England, 1975).

7 E. Leader, U. Maor, Phys. Lett. 43B, 505 (1973). R.E. Hendrick et al, Phys. Rev. D11, 536 (1975).

8 R.P. Feynman, private communication to P. Franzini, April 19, 1973.

9 J. Pumplin, Phys. Rev. D8, 2899 (1973).

10 S.D. Ellis, A.I. Sanda, Phys. Rev. D6, 1347 (1972).

11 S. Childress et al, Phys. Rev. Lett. 32, 389 (1974).

12 J. Lee-Franzini et al, Proceedings of the International Conference on High Energy Instrumentation, Frascati, Italy (1973), p. 454, edited by S. Stipcich (Laboratori Nazionali del Comitato Nazionale per l'Energia Nucleare, Frascati, Italy, 1973).

[13] R.D. Schamberger, Jr. et al, Phys. Rev. Lett. 34, 1121 (1975) and Ref. 11.

[14] P. Franzini et al, Proceedings of the International Conference on High Energy Instrumentation, Frascati, Italy (1973), pp. 505, 627, edited by S. Stipcich (Laboratori Nazionali del Comitato Nazionale per l'Energia Nucleare, Frascati, Italy, 1973).

[15] S. Childress, Ph.D. Thesis, Columbia University, (Preprint), Nevis Report 216 (1976).

[16] C. Ankenbrandt et al, submitted to the XVIIIth International Conference on High Energy Physics, Tbilisi, USSR, July 15-21, 1976.

[17] G. Barbiellini et al, Phys. Lett. 39B, 663 (1972); A. Bohm et al, Phys. Lett. 49B, 491 (1974).

[18] M.G. Albrow et al, Nucl. Phys. B54, 6 (1973); B51, 388 (1973); B72, 376 (1974); and PPF-PRINT-76-0238 (CERN Preprint, March 1976).

[19] K. Abe et al, Phys. Rev. Lett. 31, 1527 (1973); Phys. Rev. Lett. 31, 1530 (1973).

[20] D.S. Ayres et al, Phys. Rev. Lett. 37, 1724 (1976).

[21] V. Bartenev et al, Phys. Lett. 51B, 299 (1974); Y. Akimov et al, contributed paper to the XVIIth International Conference on High Energy Physics, London, 1974, NAL Report No. NAL-Conf. 74/56-Exp., and Phys. Rev. Lett. 35, 766 (1975).

[22] See for example, J.W. Chapman et al, Phys. Rev. Lett. 32, 257 (1974); S.J. Barish et al, Phys. Rev. Lett. 31, 1080 (1973); or F.T. Dao et al, Phys. Lett. 45B, 399 (1973).

[23] S. Childress et al., Phys. Lett. 65B, 177 (1976)

[24] V. Bartenev et al., Phys. Rev. Lett. 31, 1088 (1073) and Ref. 7.

[25] R. D. Schamberger Jr., Ph. D. Thesis, SUNY at Stony Brook, December 1976 (unpublished).

Table Captions

Table I: Integrated Cross Sections vs. s

Table II: $d^2\sigma/dtdM^2$ at $s = 262\ GeV^2$

Table III: " at $s = 309\ GeV^2$

Table IV: " at $s = 366\ GeV^2$

Table V: " at $s = 565\ GeV^2$

Table VI: " at $s = 741\ GeV^2$

Table 1

s GeV^2 / fraction η	262	309	366	565	741
0.10	2.00 ±0.028	2.06 ±0.028	2.03 ±0.028	2.02 ±0.028	2.16 ±0.030
0.06	1.57 ±0.026	1.60 ±0.026	1.59 ±0.026	1.65 ±0.026	1.72 ±0.027
0.04	1.31 ±0.024	1.33 ±0.024	1.33 ±0.024	1.42 ±0.024	1.49 ±0.024
0.02	0.93 ±0.022	0.95 ±0.022	0.96 ±0.022	1.11 ±0.022	1.18 ±0.022
0.01	0.60 ±0.020	0.62 ±0.020	0.64 ±0.020	0.82 ±0.020	0.90 ±0.020

$$\sigma = \int_{0.024}^{0.234} dt \int_{th}^{\eta s+m_p^2} dM^2 \left(\frac{d^2\sigma}{dt\,dM^2}\right)$$

Table 2

S = 262 GeV^2	(T=19)	(T=40)	(T=70)	(T=105)	T(MeV)
		$\frac{d^2\sigma}{dtdM^2}$ ($\frac{\mu barns}{GeV^4}$)			
M^2	-0.036	-0.075	-0.131	-0.197	t(GeV/c)^2
-25				0± 8	
-15			8±12	2 4	
- 9.5			14 14	8 8	
- 8.5			-10 15	9 8	
-7.5		-40±56	- 6 15	4 7	
-6.5		- 4 32	22 17	- 1 9	
-5.5		- 4 26	1 18	- 3 9	
-4.5		18 22	7 18	- 5 8	
-3.5		15 20	-14 16	- 2 8	
-2.5		-11 18	8 14	19 8	
-1.5		8 17	- 4 14	23 7	
-0.875	24± 77	0 20	1 19	39 8	
-0.625	25 60	5 19	- 4 18	47 9	
-0.375	45 56	13 21	14 18	52 10	
-0.125	35 54	22 26	17 17	57 11	
0.125	95 72	44 32	49 21	70 12	
0.375	170 89	65 39	65 29	85 14	
0.625	313 107	114 46	107 29	111 17	
0.875	506 121	201 54	152 35	189 20	
1.125	876 107	381 46	259 31	252 18	
1.375	1553 89	738 39	412 28	323 15	
1.625	2750 72	1286 32	606 21	383 14	
1.875	4109 56	1940 26	814 17	439 12	
2.125	4291 54	2172 22	1066 16	496 10	
2.375	3661 56	2131 21	1106 17	542 9	
2.625	3033 58	1964 21	1101 16	560 7	
2.875	2624 61	1759 20	1056 15	547 7	
3.125	2054 62	1495 21	957 15	533 7	
3.375	1530 63	1225 21	846 15	516 7	
3.625	1285 59	984 21	763 16	487 7	
3.875	1229 57	865 22	700 18	453 7	
4.25	1132 48	765 20	606 18	412 8	
4.75	1156 49	703 22	516 19	354 9	
5.25	1028 57	675 20	435 19	330 8	
5.75	987 58	656 20	376 18	305 8	
6.25	994 55	575 20	348 17	264 8	
6.75	892 51	502 20	339 16	226 8	
7.25	877 48	454 21	342 17	201 8	
7.75	736 50	392 22	342 18	196 8	
8.25	747 51	408 21	330 18	188 8	
8.75	729 49	448 19	285 17	172 8	
9.25	542 47	423 19	281 16	160 9	
9.75	557 46	389 21	269 15	159 9	
10.5	622 38	339 18	222 14	143 8	
11.5	613 38	327 18	234 15	121 8	
12.5	563 39	340 18	219 17	117 9	
13.5	588 39	273 17	206 17	126 9	
14.5	491 39	261 18	182 17	127 10	
15.5	344 40	296 19	190 16	114 10	
16.5	394 44	285 19	203 18	82 9	
17.5	461 52	227 19	172 20	83 9	
18.5	494 62	263 19	142 17	116 9	
19.5	495 68	293 19	122 17	128 10	
21	397 64	313 19	146 17	115 10	
23	332 79	280 25	154 20	103 16	
25	288 107	209 28	170 24	98 14	
27		210 31	103 24	93 13	
29		124 37	134 27	130 18	
31		139 47	106 27	85 25	
33		261 57	107 30	118 23	
35			85 33	140 21	
37			63 42	101 20	
39			98 56	45 22	
42.5				42 25	

Table 3

S = 309 GeV^2	(T=19)	(T=40)	(T=70)	(T=105)	T(MeV)
		$\frac{d^2\sigma}{dtdM^2}$ ($\frac{\mu barns}{GeV^4}$)			
M^2	-0.036	-0.075	-0.131	-0.197	t(GeV/c)^2
-25				9± 4	
-15			-7± 7	-1 3	
- 9.5			3 10	5 5	
- 8.5		24±28	9 10	1 5	
- 7.5		-4 20	11 11	4 5	
- 6.5		-4 17	-4 11	14 5	
- 5.5		6 15	2 11	10 5	
- 4.5		-4 13	0 10	2 5	
- 3.5		-5 12	15 9	20 5	
- 2.5		1 12	4 9	42 5	
- 7.5	13± 53	3 11	27 9	60 6	
- 0.875	-7 41	18 13	58 11	68 7	
- 0.625	2 37	19 12	65 10	69 9	
- 0.375	30 35	15 13	68 10	66 11	
- 0.125	54 41	48 16	78 12	73 13	
0.125	82 49	75 20	54 14	84 16	
0.375	118 60	101 23	70 17	108 18	
0.625	188 70	136 26	78 19	144 20	
0.875	439 81	223 30	126 21	200 21	
1.125	726 70	382 27	220 19	246 20	
1.375	1342 60	609 23	317 17	285 18	
1.625	2274 49	970 20	454 14	341 17	
1.875	3693 41	1543 17	621 12	384 13	
2.125	4064 35	1949 15	838 10	420 11	
2.375	3615 36	1993 13	982 9	441 9	
2.625	2909 37	1877 13	1034 10	465 7	
2.875	2334 38	1672 13	1018 10	484 6	
3.125	1964 39	1433 13	951 9	482 4	
3.375	1592 39	1153 13	862 9	477 4	
3.625	1317 40	959 13	772 9	466 4	
3.875	1167 40	863 14	700 9	447 5	
4.25	1068 34	758 13	607 10	413 4	
4.75	1069 33	677 13	517 10	373 5	
5.25	1027 30	618 14	460 11	333 6	
5.75	915 35	549 13	426 11	296 5	
6.25	869 42	515 13	390 11	265 5	
6.75	824 37	505 12	362 10	233 5	
7.25	751 31	467 12	325 10	210 4	
7.75	724 30	437 12	315 10	195 5	
8.25	719 30	415 13	301 10	190 5	
8.75	651 31	353 13	266 10	180 5	
9.25	608 32	313 13	241 10	175 5	
9.75	580 33	325 13	244 11	167 6	
10.5	561 27	324 11	240 9	158 5	
11.5	541 26	307 11	227 9	140 6	
12.5	524 26	272 11	215 10	115 5	
13.5	502 26	270 11	190 10	109 5	
14.5	470 26	248 11	188 10	118 5	
15.5	430 25	251 11	178 10	119 6	
16.5	444 25	248 11	187 10	123 6	
17.5	394 25	235 11	189 10	119 6	
18.5	366 27	234 11	161 11	101 6	
19.5	396 29	227 12	157 11	90 6	
21	371 29	200 10	149 9	92 5	
23	355 37	206 10	128 10	87 5	
25	389 42	223 13	145 10	84 6	
27	417 50	201 16	149 11	88 8	
29	354 67	201 18	141 13	99 9	
31	415 115	184 19	123 19	87 9	
33		194 21	141 20	69 10	
35		170 25	125 19	87 10	
37		143 30	117 20	87 11	
39		112 37	156 23	82 12	
42.5		158 57	110 21	71 11	
47.5			170 33	60 17	

Table 4

$s = 366$ GeV^2	(T=19)	(T=40)	(T=70)	(T=105)	T(MeV)
		$\frac{d^2\sigma}{dtdM^2}$ ($\frac{\mu barns}{GeV^4}$)			
M^2	-0.036	-0.075	-0.131	-0.197	t(GeV/c)^2
-35				8± 6	
-25				3 3	
-15		30±32	3± 5	2 3	
- 9.5		-20 20	-1 9	4 4	
- 8.5		- 6 17	3 10	4 4	
- 7.5		11 14	10 10	0 4	
- 6.5		15 13	4 10	2 4	
- 5.5		1 12	-2 9	8 4	
- 4.5		-1 11	3 8	18 4	
- 3.5		12 12	15 8	33 4	
- 2.5		-2 11	12 9	47 4	
- 1.5	-38± 41	6 11	28 8	65 5	
- 0.875	-14 33	5 12	50 10	72 6	
- 0.625	14 30	23 12	43 9	77 8	
- 0.375	36 30	31 11	46 12	77 10	
- 0.125	84 32	41 14	50 16	89 12	
0.125	80 44	73 20	20 70	108 14	
0.375	138 54	102 25	120 24	136 16	
0.625	258 65	117 30	144 26	161 18	
0.875	387 75	230 35	191 31	205 20	
1.125	671 66	292 30	240 27	237 18	
1.375	997 55	445 25	304 24	278 16	
1.625	1823 46	679 20	381 19	315 14	
1.875	2921 35	1027 14	522 17	340 12	
2.125	3521 31	1544 12	710 12	366 10	
2.375	3433 31	1809 12	854 9	381 8	
2.625	2932 31	1765 12	937 8	397 6	
2.875	2493 32	1611 12	925 8	409 5	
3.125	2056 33	1401 12	877 8	411 3	
3.375	1636 33	1178 12	814 8	411 4	
3.625	1391 33	1007 12	745 8	410 4	
3.875	1214 35	869 12	681 8	404 4	
4.25	1107 34	762 12	614 8	389 4	
4.75	958 33	662 12	520 9	354 4	
5.25	851 31	623 12	453 9	322 4	
5.75	814 29	548 12	390 9	294 5	
6.25	774 28	465 13	367 10	265 5	
6.75	733 33	441 13	342 10	243 4	
7.25	751 38	429 12	302 9	227 4	
7.75	651 35	397 12	276 9	210 4	
8.25	572 32	416 12	257 9	199 4	
8.75	561 32	388 12	265 8	180 4	
9.25	565 31	354 12	262 8	165 4	
9.75	549 31	316 13	259 9	154 4	
10.5	468 27	291 12	229 9	144 4	
11.5	486 25	276 12	200 9	139 5	
12.5	443 24	260 12	191 8	133 5	
13.5	430 24	233 11	176 8	127 5	
14.5	436 23	223 11	167 8	116 5	
15.5	474 23	233 11	173 9	101 5	
16.5	411 24	221 11	169 9	90 5	
17.5	373 23	215 11	153 9	84 5	
18.5	343 23	219 12	128 9	89 5	
19.5	340 23	203 11	123 9	88 5	
21.	344 20	208 11	138 8	82 5	
23.	332 23	183 11	128 8	66 4	
25.	327 29	174 11	113 8	72 4	
27.	300 34	203 11	126 9	89 5	
29.	296 38	167 12	105 10	79 6	
31.	270 44	142 15	91 12	84 7	
33.	259 57	185 18	128 15	84 9	
35.	213 68	184 18	119 16	80 12	
37.	270 115	168 19	146 17	77 12	
39.		129 20	122 18	70 9	
42.5		113 24	111 13	69 8	
47.5			111 17	71 11	
52.5				50 11	
57.5				19 20	

Table 5

S = 565 GeV^2	(T=19)		(T=40)		(T=70)		(T=105)		T(MeV)
			$\frac{d^2\sigma}{dtdM^2}(\frac{\mu barns}{GeV^4})$						
M^2	-0.036		-0.075		-0.131		-0.197		t(GeV/c)^2
-45.							2±	1	
-35.					7±	6	1	1	
-25.					-4	2	1	1	
-15.			-8±	4	-7	1	1	1	
- 9.5			-1	5	-8	3	3	2	
- 8.5			-2	5	0	2	4	2	
- 7.5			-1	5	4	2	4	2	
- 6.5	-45±	148	-4	5	3	2	10	2	
- 5.5	90	106	-4	5	5	3	15	2	
- 4.5	-34	35	-3	6	10	3	20	2	
- 3.5	14	20	-3	6	21	3	25	2	
- 2.5	13	14	4	5	40	3	41	3	
- 1.5	9	11	42	5	64	3	71	4	
- 0.875	18	11	27	5	70	3	92	5	
- 0.625	48	10	32	5	75	4	108	7	
- 0.375	52	9	76	6	75	5	122	8	
- 0.125	89	11	78	8	85	6	143	8	
0.125	142	14	137	9	116	7	163	9	
0.375	234	17	124	11	166	8	171	10	
0.625	359	20	198	12	251	9	188	11	
0.875	565	22	345	14	333	10	203	13	
1.125	889	20	546	12	442	9	220	12	
1.375	1323	17	846	11	546	8	237	10	
1.625	1893	14	1154	9	628	7	247	9	
1.875	2388	11	1435	8	710	6	257	8	
2.125	2656	9	1560	6	754	5	270	7	
2.375	2715	10	1584	5	774	4	272	6	
2.625	2537	10	1493	5	774	3	279	5	
2.875	2269	10	1360	5	762	2	277	5	
3.125	1895	10	1168	4	738	2	274	4	
3.375	1625	10	1049	5	700	3	272	3	
3.625	1354	10	914	5	651	3	267	3	
3.875	1171	11	825	5	607	3	266	2	
4.25	1014	12	730	5	553	3	258	2	
4.75	839	12	615	6	467	3	251	2	
5.25	753	13	539	6	410	3	239	1	
5.75	678	12	489	6	360	3	235	1	
6.25	602	12	441	6	321	3	219	1	
6.75	559	12	404	6	296	3	205	1	
7.25	507	11	368	6	274	3	192	1	
7.75	491	12	345	6	255	3	181	1	
8.25	460	11	326	6	243	3	169	1	
8.75	433	11	307	6	224	3	163	1	
9.25	422	11	283	6	213	3	153	1	
9.75	418	12	261	6	201	3	144	1	
10.5	388	12	237	6	187	3	130	1	
11.5	359	12	225	8	167	3	114	1	
12.5	324	13	209	7	150	3	104	1	
13.5	282	12	195	6	135	3	94	1	
14.5	272	12	186	7	136	3	85	1	
15.5	262	13	171	6	131	3	79	1	
16.5	275	14	155	6	122	3	75	1	
17.5	251	12	146	6	120	3	73	1	
18.5	228	10	149	5	109	3	69	1	
19.5	222	10	150	6	102	3	69	1	
21.	203	9	142	5	95	3	67	1	
23.	210	9	124	5	90	3	62	1	
25.	208	10	117	5	80	3	60	1	
27.	180	9	112	4	84	3	58	1	
29.	173	9	106	5	78	3	58	2	
31.	168	9	105	5	76	3	59	2	
33.	138	9	112	6	74	3	54	2	
35.	139	10	101	6	77	3	49	1	
37.	163	11	98	4	82	3	47	1	
39.	173	13	98	4	66	3	46	2	
42.5	142	12	86	4	66	2	47	2	
47.5	153	15	78	6	71	2	45	2	
52.5	172	24	72	7	68	5	40	2	
57.5			82	8	64	5	44	5	
62.5			88	9	63	4	52	2	
67.5			99	11	75	6	50	3	
72.5			134	20	72	5	62	3	
77.5					71	10	57	3	
82.5					73	9	75	7	
87.5							65	5	
92.5							55	12	

Table 6

S = 741 GeV^2	(T=19)	(T=40)	(T=70)	(T=105)	T(MeV)
		$\frac{d^2\sigma}{dtdM^2}$ ($\frac{\mu barns}{GeV^4}$)			
M^2	-0.036	-0.075	-0.131	-0.197	t(GeV/c)^2
-65.				0± 5	
-55.				0 2	
-45.				-1 2	
-35.			0± 5	-1 2	
-25.			-4 3	1 2	
-15.		-8± 7	-9 4	5 2	
- 9.5		-18 8	-3 5	7 2	
- 8.5		-10 8	8 5	9 2	
- 7.5		- 7 8	15 5	11 2	
- 6.5		- 4 8	7 6	12 2	
- 5.5	26±78	- 2 8	-4 5	20 2	
- 4.5	-9 46	4 8	12 5	30 2	
- 3.5	13 37	4 8	37 5	50 3	
- 2.5	21 31	42 7	66 5	79 3	
- 1.5	50 23	82 6	91 6	117 5	
- 0.875	83 22	86 6	104 5	141 7	
- 0.625	126 22	78 7	112 6	154 8	
- 0.375	156 23	88 8	117 7	168 10	
- 0.125	199 25	104 9	144 7	179 11	
0.125	246 29	155 10	173 8	186 13	
0.375	362 33	203 12	218 9	188 14	
0.625	459 38	330 14	267 10	203 16	
0.875	611 43	461 15	327 11	207 18	
1.125	792 38	580 14	416 10	222 16	
1.375	1088 33	771 12	472 9	219 14	
1.625	1461 29	969 10	550 8	225 13	
1.875	1873 24	1114 9	577 7	231 11	
2.125	2202 21	1242 8	623 7	231 10	
2.375	2270 20	1343 7	644 6	233 8	
2.625	2189 19	1347 7	659 5	237 6	
2.875	1996 19	1306 7	632 5	236 5	
3.125	1790 19	1220 7	607 5	243 3	
3.375	1585 20	1121 7	566 4	241 3	
3.625	1409 20	1003 7	548 4	207 3	
3.875	1264 21	888 7	535 4	186 2	
4.25	1114 21	772 7	499 4	183 2	
4.75	931 22	631 8	444 5	186 2	
5.25	775 26	540 8	391 5	183 2	
5.75	630 28	463 8	357 5	181 2	
6.25	491 26	428 8	316 5	190 3	
6.75	449 25	395 8	288 5	183 3	
7.25	426 22	347 8	272 5	176 2	
7.75	462 22	308 8	246 5	164 3	
8.25	452 19	280 8	236 5	156 3	
8.75	421 19	258 7	220 5	147 2	
9.25	353 19	257 9	209 5	144 3	
9.75	292 21	232 8	198 5	139 2	
10.5	327 22	208 7	182 5	132 3	
11.5	421 22	213 9	159 5	115 2	
12.5	374 25	210 8	134 5	96 3	
13.5	300 25	197 8	118 5	86 2	
14.5	270 20	183 8	122 5	79 2	
15.5	231 18	162 9	113 5	75 2	
16.5	255 20	153 9	107 5	70 2	
17.5	301 21	128 8	106 5	65 3	
18.5	238 22	118 9	102 5	67 3	
19.5	125 24	111 8	96 5	66 3	
21.	137 18	126 7	96 5	64 3	
23.	150 19	137 8	86 5	56 3	
25.	179 20	139 9	68 5	49 3	
27.	154 17	94 8	62 4	48 4	
29.	156 17	81 6	73 5	42 3	
31.	207 17	84 7	76 5	40 3	
33.	170 17	140 8	57 6	44 3	
35.	164 16	109 8	57 5	48 3	
37.	166 17	64 8	57 5	43 3	
39.	138 17	81 7	60 5	40 4	
42.5	134 14	80 6	65 5	39 4	
47.5	136 17	50 6	52 5	36 3	
52.5	141 24	61 6	64 4	42 3	
57.5	146 29	66 7	50 5	31 4	
62.5	172 36	94 10	47 5	32 4	
67.5		102 12	87 10	49 6	
72.5		116 13	50 8	41 7	
77.5		83 15	72 8	44 7	
82.5		88 17	53 10	47 6	
87.5		83 19	30 12	27 6	
92.5		88 32	41 12	11 8	
97.5			38 12	29 10	
105.			30 12	29 7	
115.			35 23	14 10	

Figure Captions

Fig. 1 A schematic diagram of our experimental setup.

Fig. 2a The theoretical range-energy correlation curve for four particles (pions, protons, deuterons and tritons) in our experimental apparatus.

2b Scatter plot of E_1 vs. E_2 for $\sim 10^6$ recoil particles. π mesons are barely visible above background. The insert is a plot of the number of events vs. mass of the particle showing our excellent particle separation and indicating the low accidental background levels.

Fig. 3 Electronic channel for a telescope from detector to sample and hold, including discriminator and deadtime scalers.

Fig. 4 Block diagram of flag scan, analog multiplexer and analog to digital conversion.

Fig. 5 Event analyzer block diagram. The memory output for "proton down" case is shown.

Fig. 6 A typical plot of $d^2\sigma/dtdM^2$ showing our good mass resolution and large mass range.

Fig. 7 A plot of the differential cross section showing the unambiguous separation of elastic and inelastic data at low energy.

Fig. 8 Plots of $d^2N/dtd\Omega$ showing the fitted form (dashed line) used to separate elastic and inelastic data at three different values of T_{el}. Solid lines represent elastic contributions.

Fig. 9 A plot of dN_{el}/dt for a small set of data at p = 300 GeV/c with a fit over two t intervals to the form Ae^{bt}.

Fig. 10 b(s) vs. s for two t intervals. The low t interval has been corrected for a t dependent solid angle using data at $s \sim 350$ GeV^2.

Fig. 11 A plot of the low mass peak showing that it is essentially independent of s for fixed M^2 (i.e., not for fixed $x = 1-M^2/s$).

Fig. 12 A plot of the high mass region showing that the cross section is tending to a constant level whose height appears to vary like 1/s. The solid lines are the values of 11/S at the indicated s. The dashed lines are obtained using the fit of Ref. 19.

Fig. 13 A plot of t dependence for 5 intervals in M^2 showing the slope is always > 6 GeV^{-2} justifying our t extrapolation independent of M^2. The dashed curve is the R-I fit at x = 0.91 extended to our t region.

Fig. 14 Fraction of $d\sigma/dt$ measured in the present experiment vs. slope parameter for a simple t dependence of the form exp(bt).

Fig. 15 A plot of integrated cross section vs. s. The solid lines in a) are the best fits to our data as explained in the text. The dashed lines in b) are the best fits requiring $\alpha = 2$, showing a clear inconsistency.

Fig. 16 A comparison of the measured spectrum at $s = 366$ GeV^2 with that predicted from the fit to our integrated cross section.

Fig. 17 A comparison of our large mass data to other experiments, showing good agreement in both slope and magnitude of the inelastic cross section.

Fig. 18 A plot of $M^2 d\sigma/dM^2$ vs. M^2 again showing that our data is inconsistent with a dominate $1/M^2$ mass dependence. Dashed area is prediction of formula of Ref. 21 including errors.

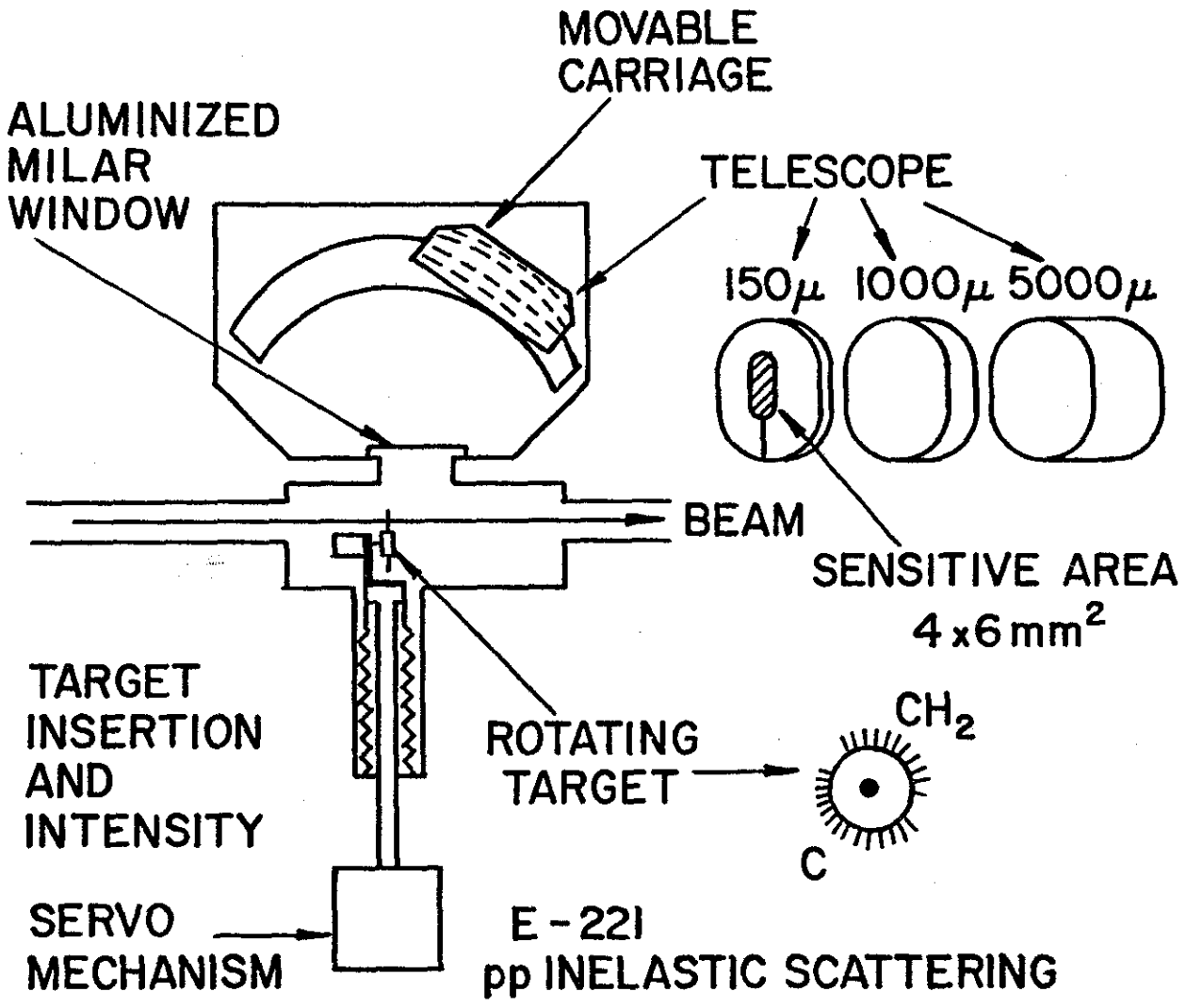
MOVABLE
CARRIAGE
ALUMINIZED
MILAR
WINDOW
TELESCOPE
150μ
1000μ
5000μ
BEAM
SENSITIVE AREA
4 x 6 mm²
TARGET
INSERTION
AND
INTENSITY
ROTATING
TARGET
CH₂
C
SERVO
MECHANISM
E - 221
pp INELASTIC SCATTERING

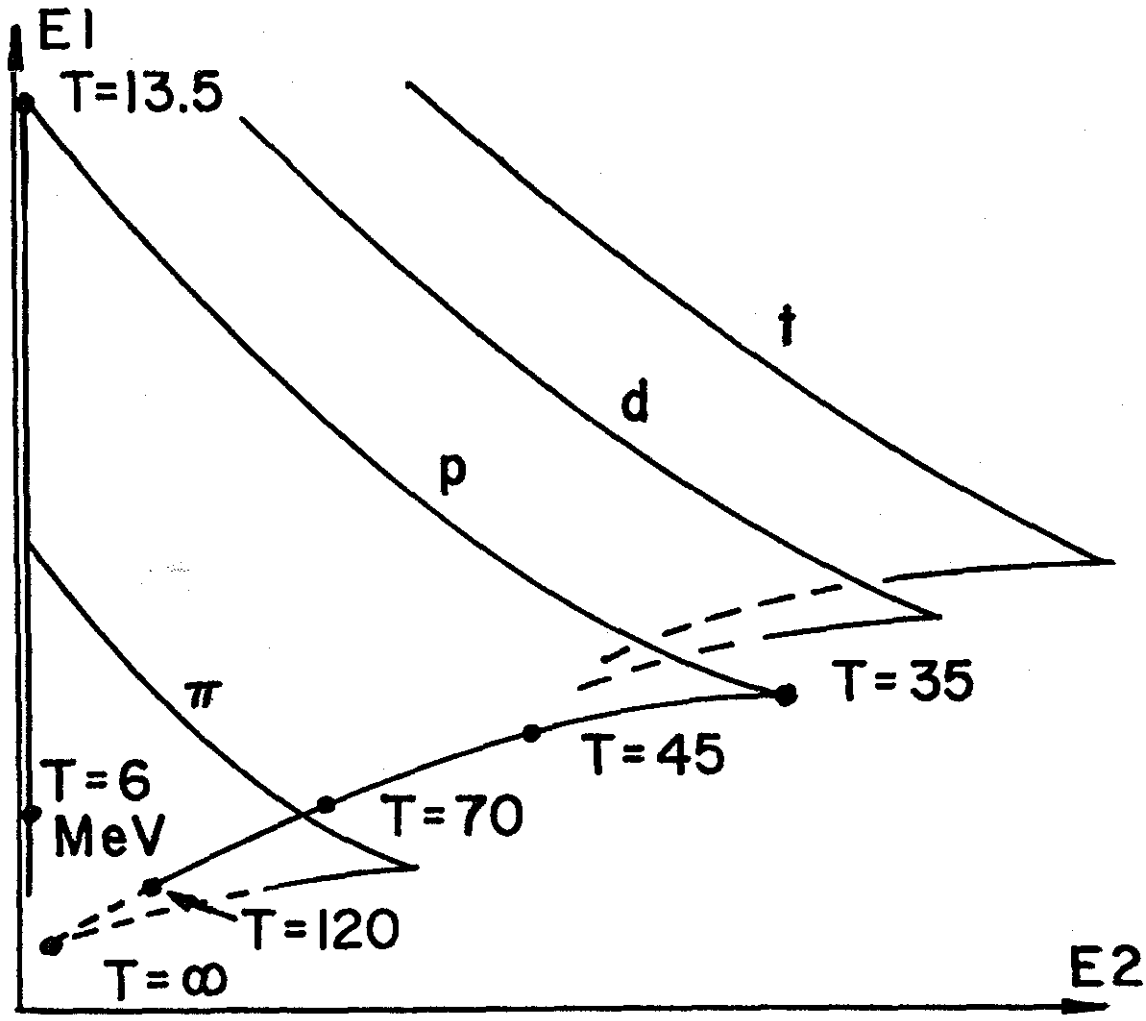
E1
T=13.5
t
d
p
π
T=35
T=45
T=70
T=6
MeV
T=120
T=∞
E2

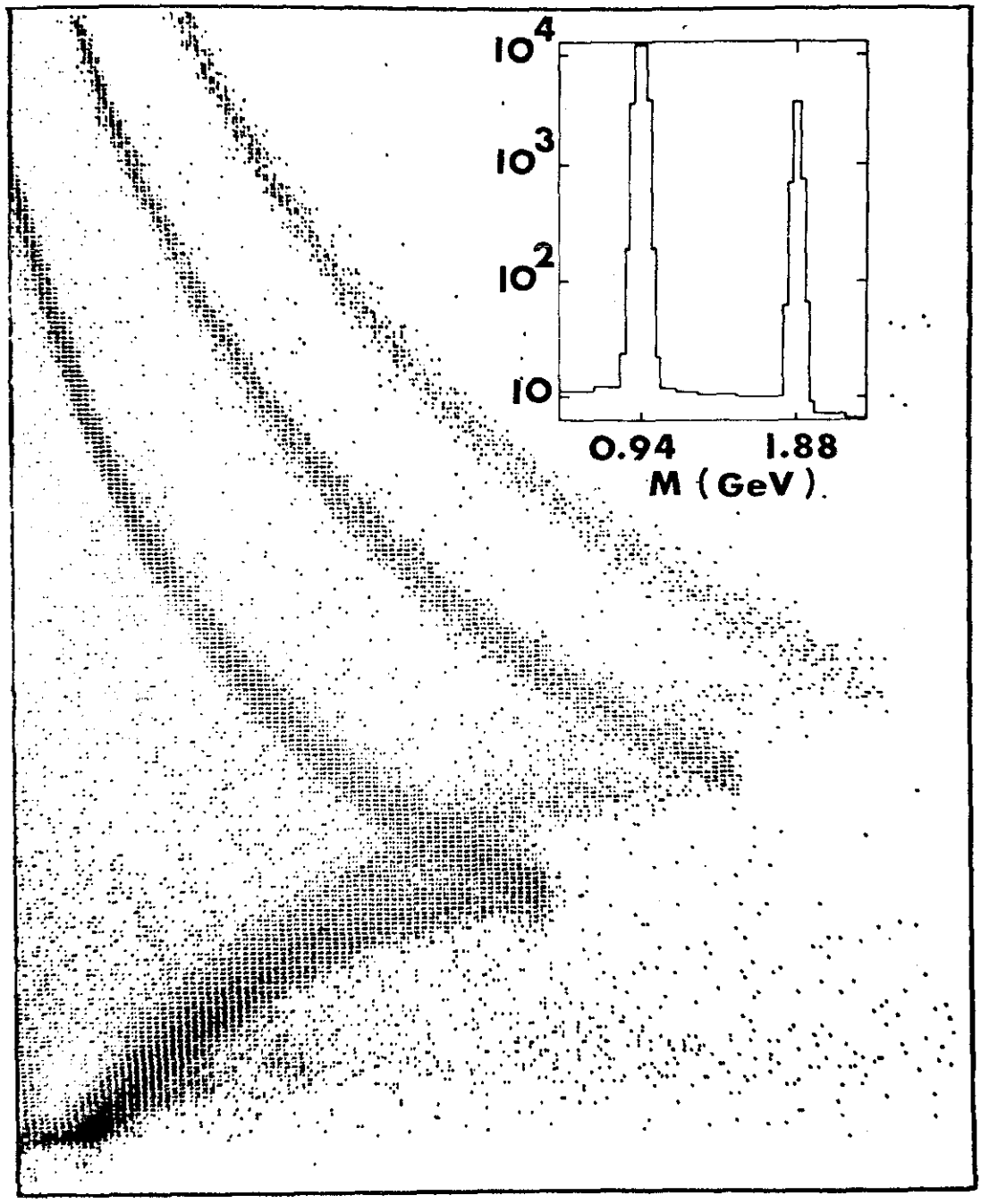
10^4
10^3
10^2
10
0.94
1.88
M (GeV)

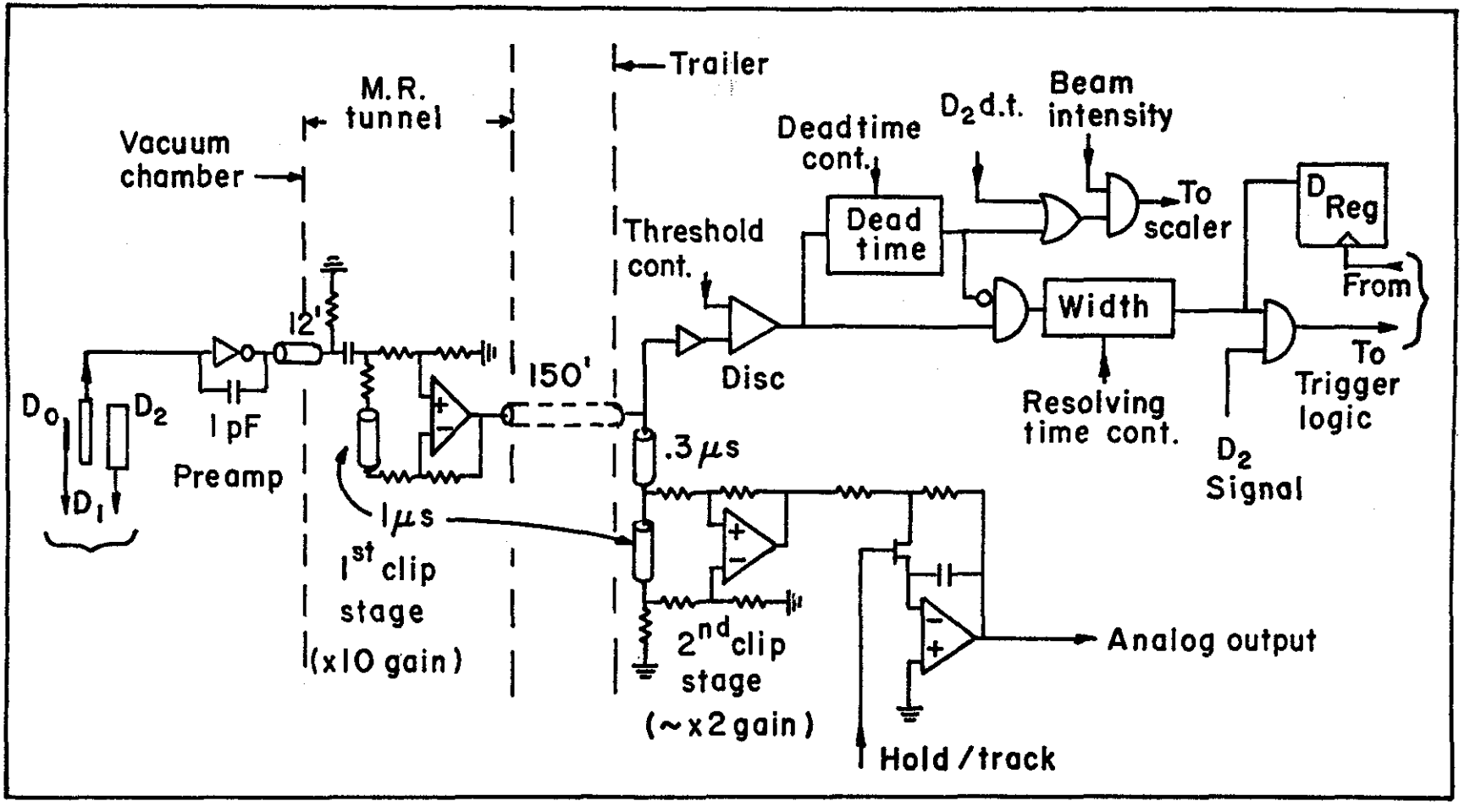
Trailer
M.R.
tunnel
Vacuum
chamber
Deadtime
cont.
D_2d.t.
Beam
intensity
To
scaler
D_{Reg}
Dead
time
Threshold
cont.
From
Width
12'
150'
Disc
To
Trigger
logic
D_0
D_2
1 pF
Preamp
Resolving
time cont.
D_2
Signal
.3 μs
D_1
1μs
1st clip
stage
(x10 gain)
2nd clip
stage
(~x2 gain)
Analog output
Hold/track

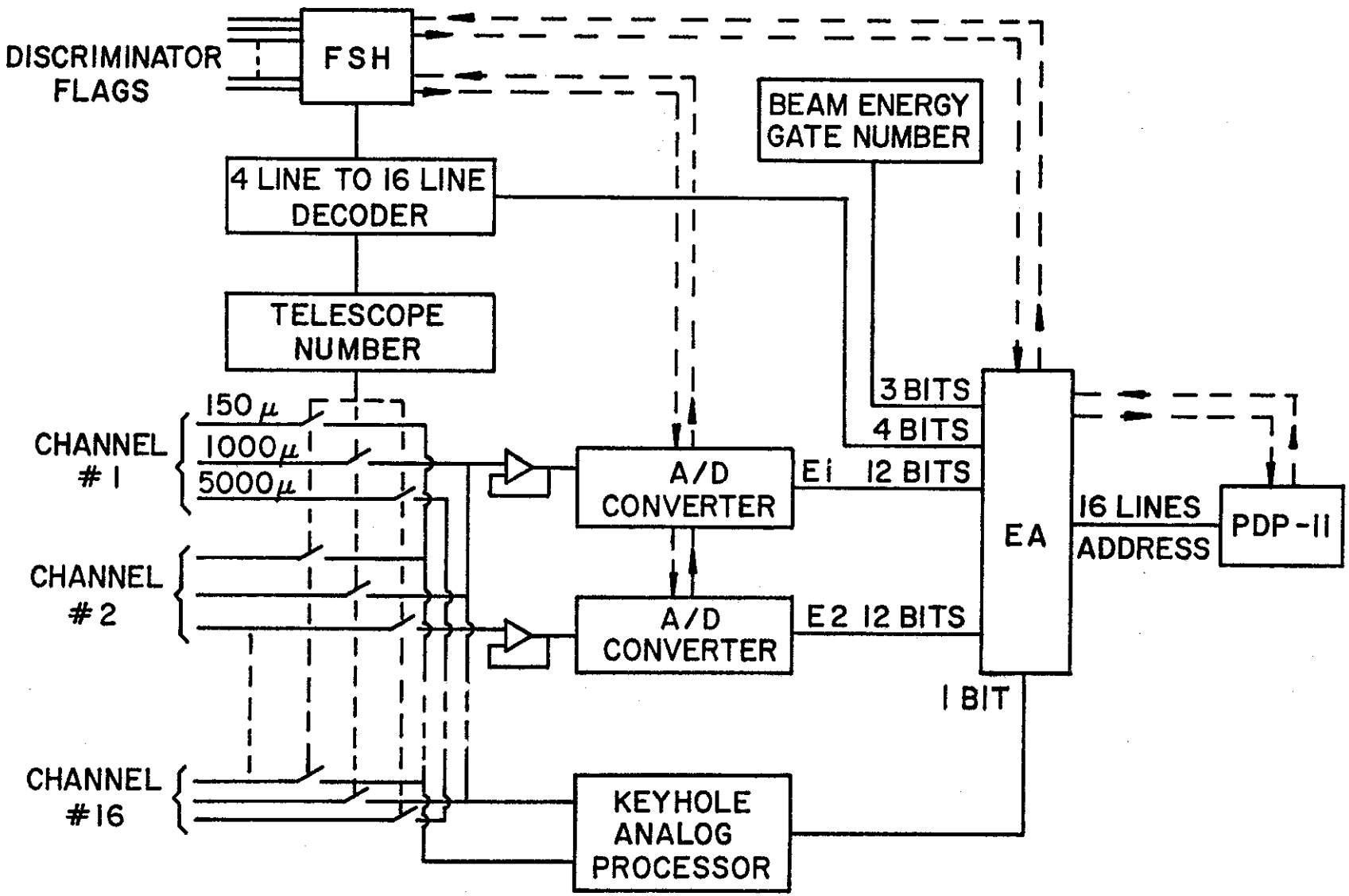
DISCRIMINATOR FLAGS
FSH
4 LINE TO 16 LINE DECODER
TELESCOPE NUMBER
BEAM ENERGY GATE NUMBER
CHANNEL #1
150 μ
1000 μ
5000 μ
CHANNEL #2
CHANNEL #16
A/D CONVERTER
A/D CONVERTER
E1 12 BITS
E2 12 BITS
3 BITS
4 BITS
EA
16 LINES
ADDRESS
PDP-11
1 BIT
KEYHOLE ANALOG PROCESSOR

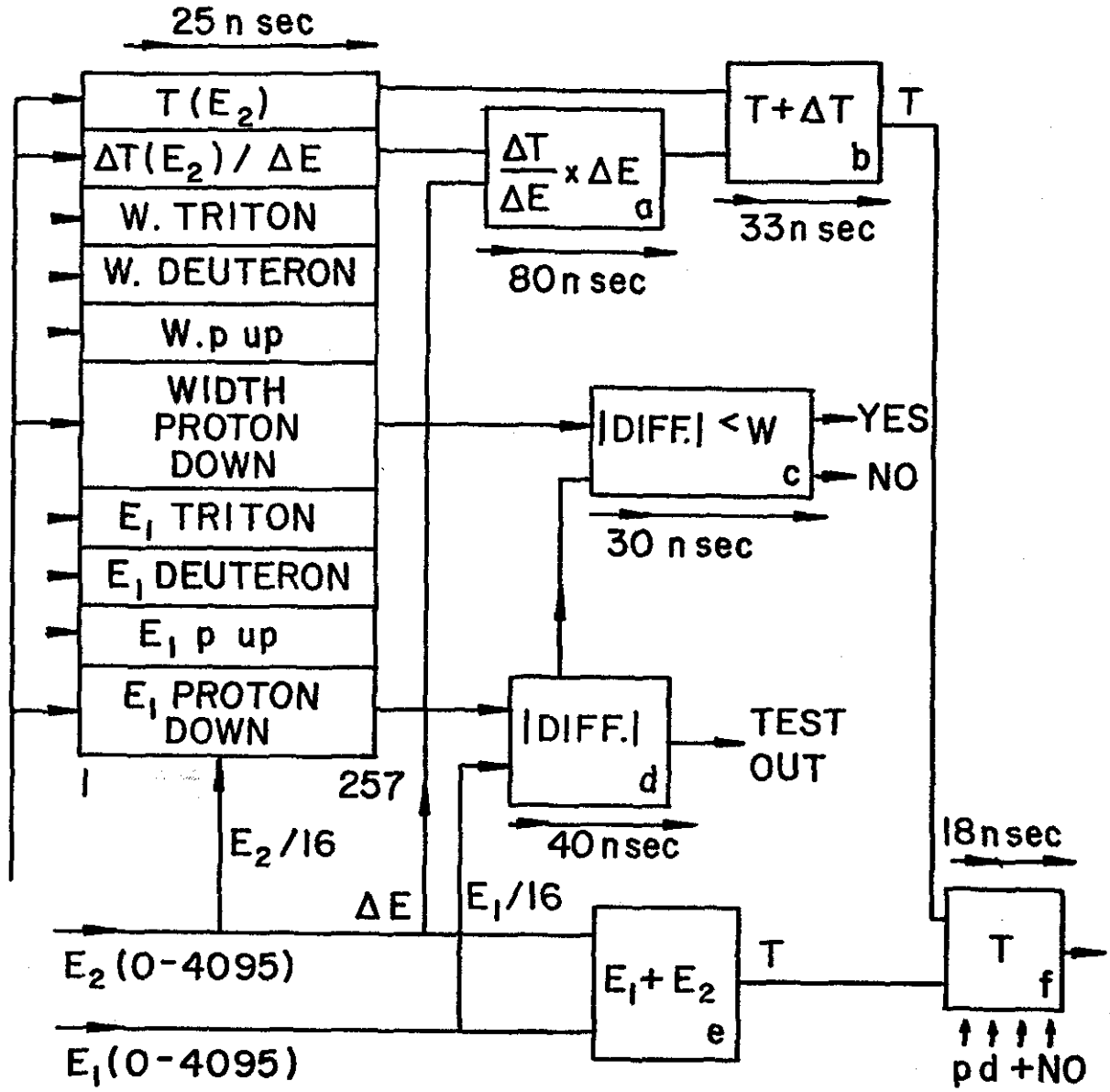

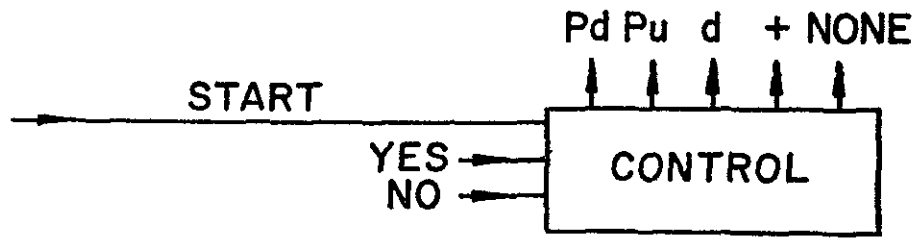

a,b,c,d,e,f ARE SEPARATE ARITHMETIC UNITS

25 +80+33+18 = 156

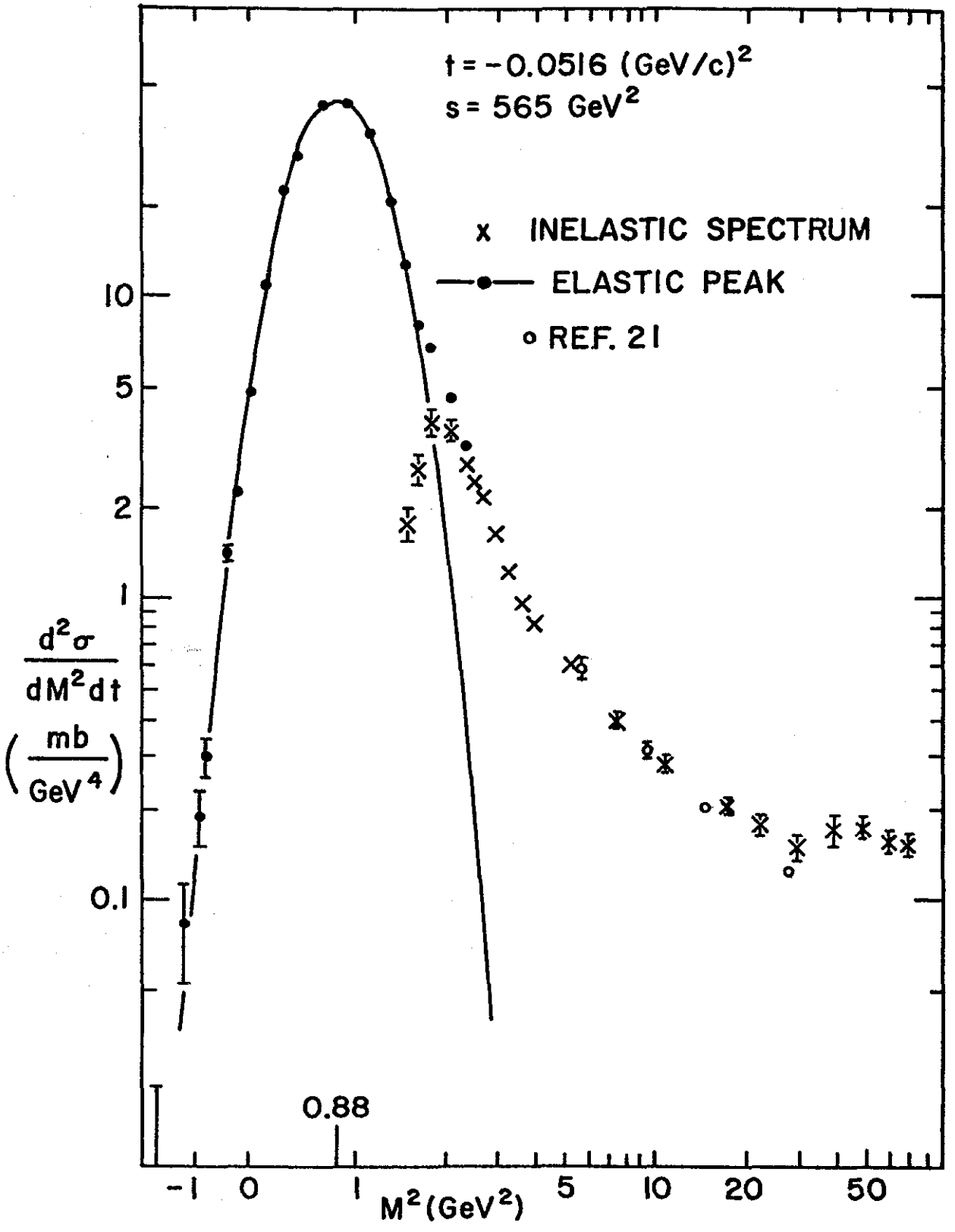
t = -0.0516 (GeV/c)²
s = 565 GeV²
x INELASTIC SPECTRUM
ELASTIC PEAK
o REF. 21
10
5
2
1
0.1
d²σ / dM²dt
(mb / GeV⁴)
0.88
-1
0
1
5
10
20
50
M² (GeV²)

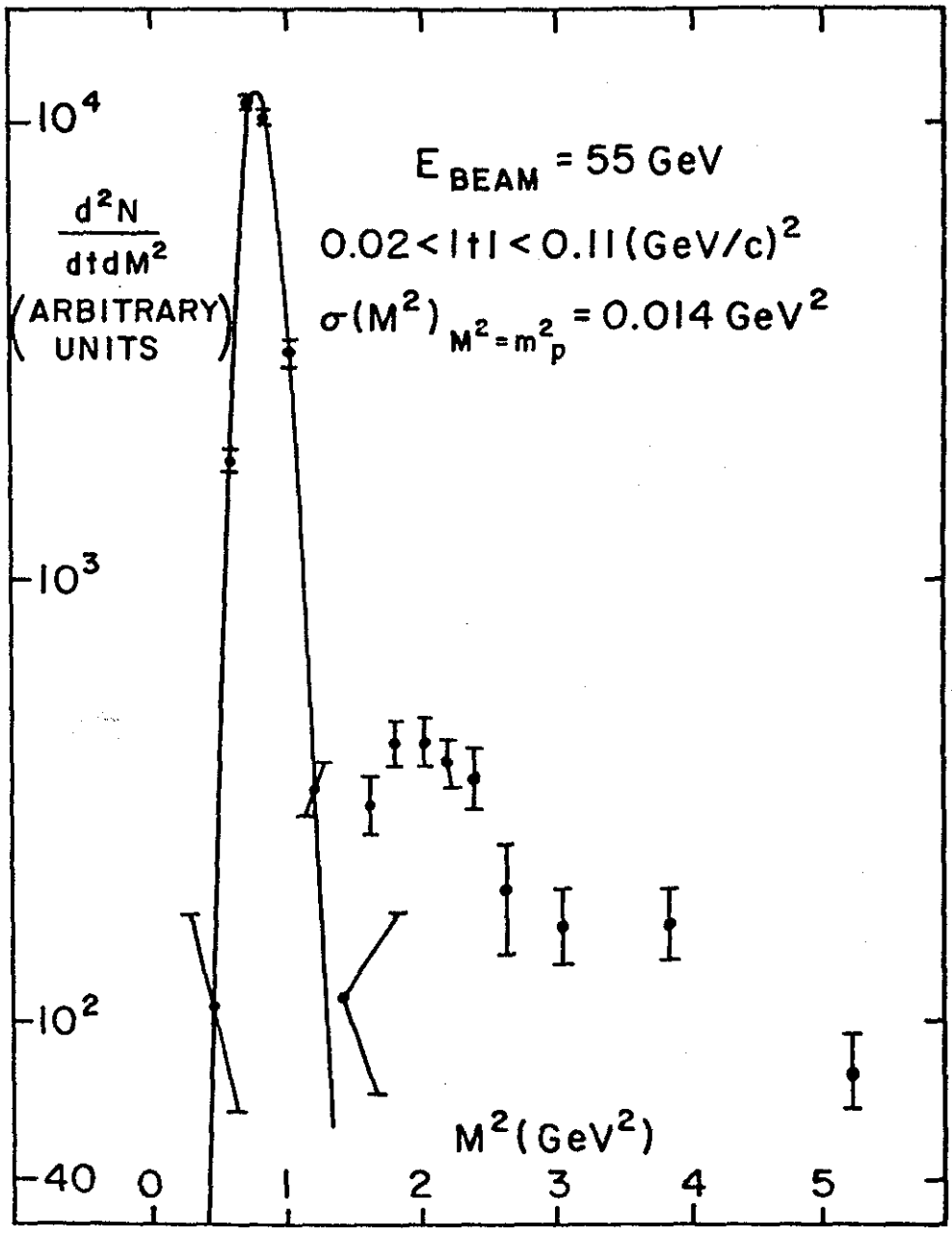
10^4
10^3
10^2
40
$\frac{d^2N}{dtdM^2}$
(ARBITRARY UNITS)
$E_{BEAM} = 55$ GeV
$0.02 < |t| < 0.11 (GeV/c)^2$
$\sigma(M^2)_{M^2=m_p^2} = 0.014$ GeV^2
M^2(GeV^2)
0
1
2
3
4
5

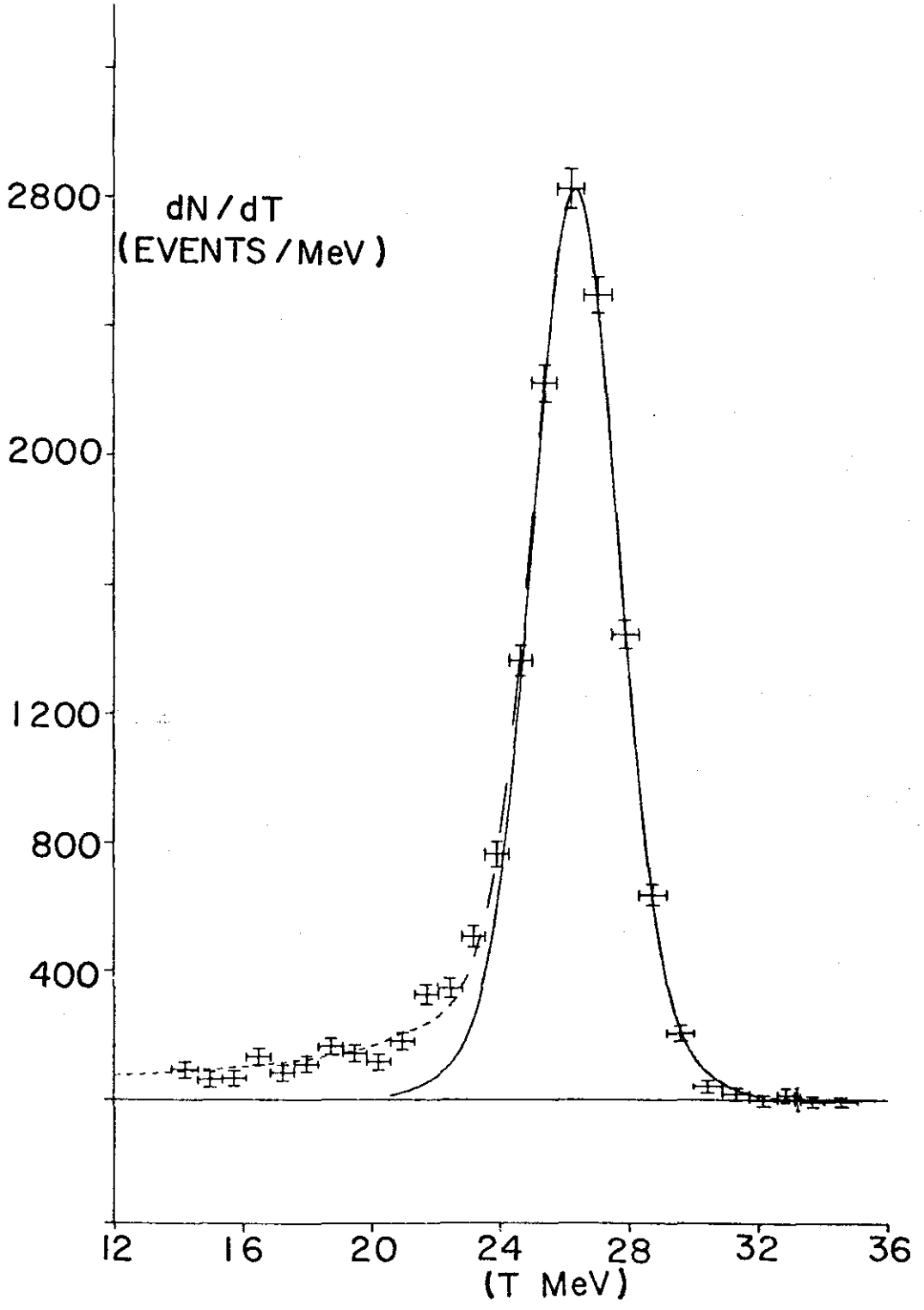
dN / dT
(EVENTS / MeV)
2800
2000
1200
800
400
12
16
20
24
28
32
36
(T MeV)

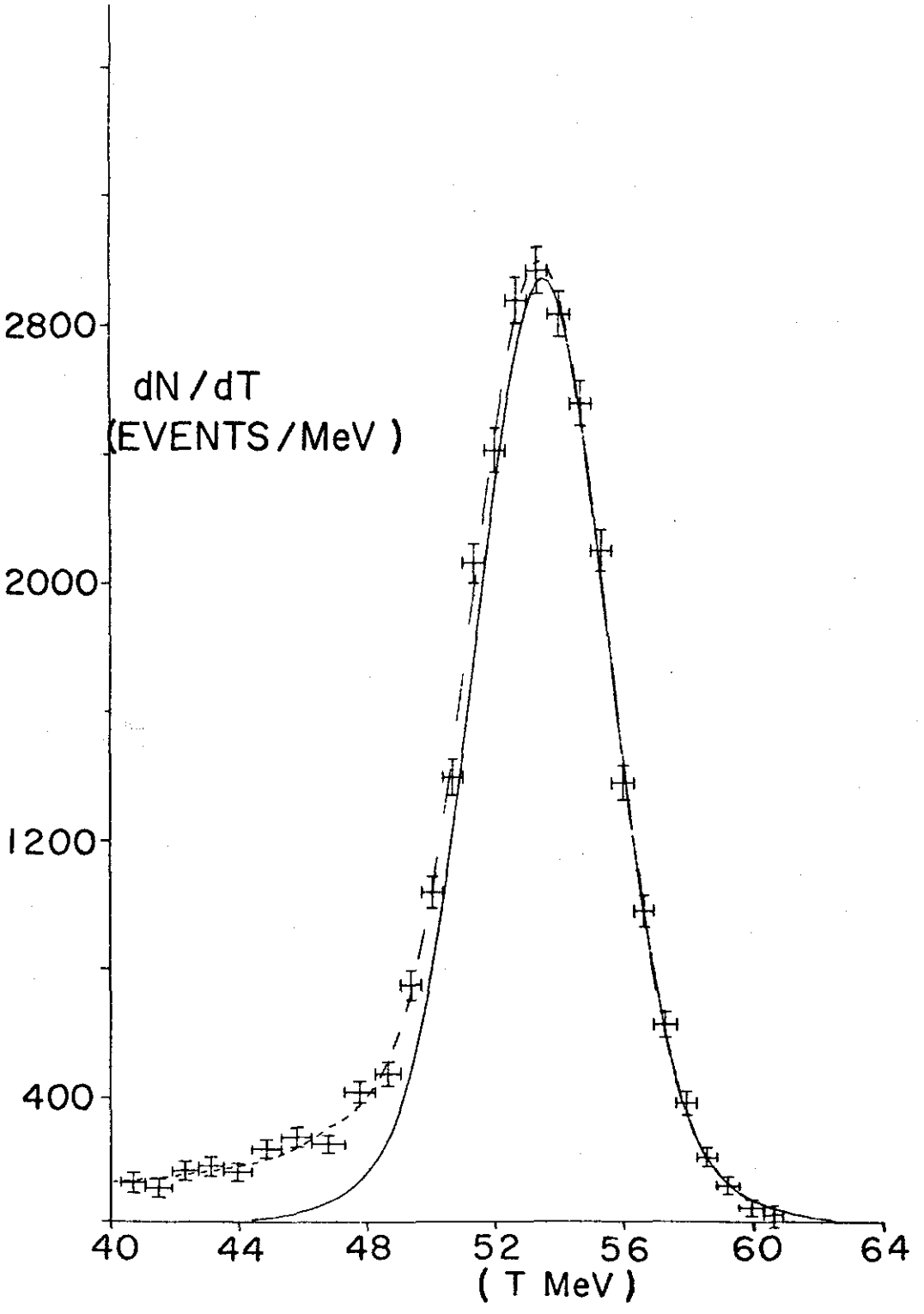
2800
2000
1200
400
dN / dT
(EVENTS / MeV)
40
44
48
52
56
60
64
(T MeV)

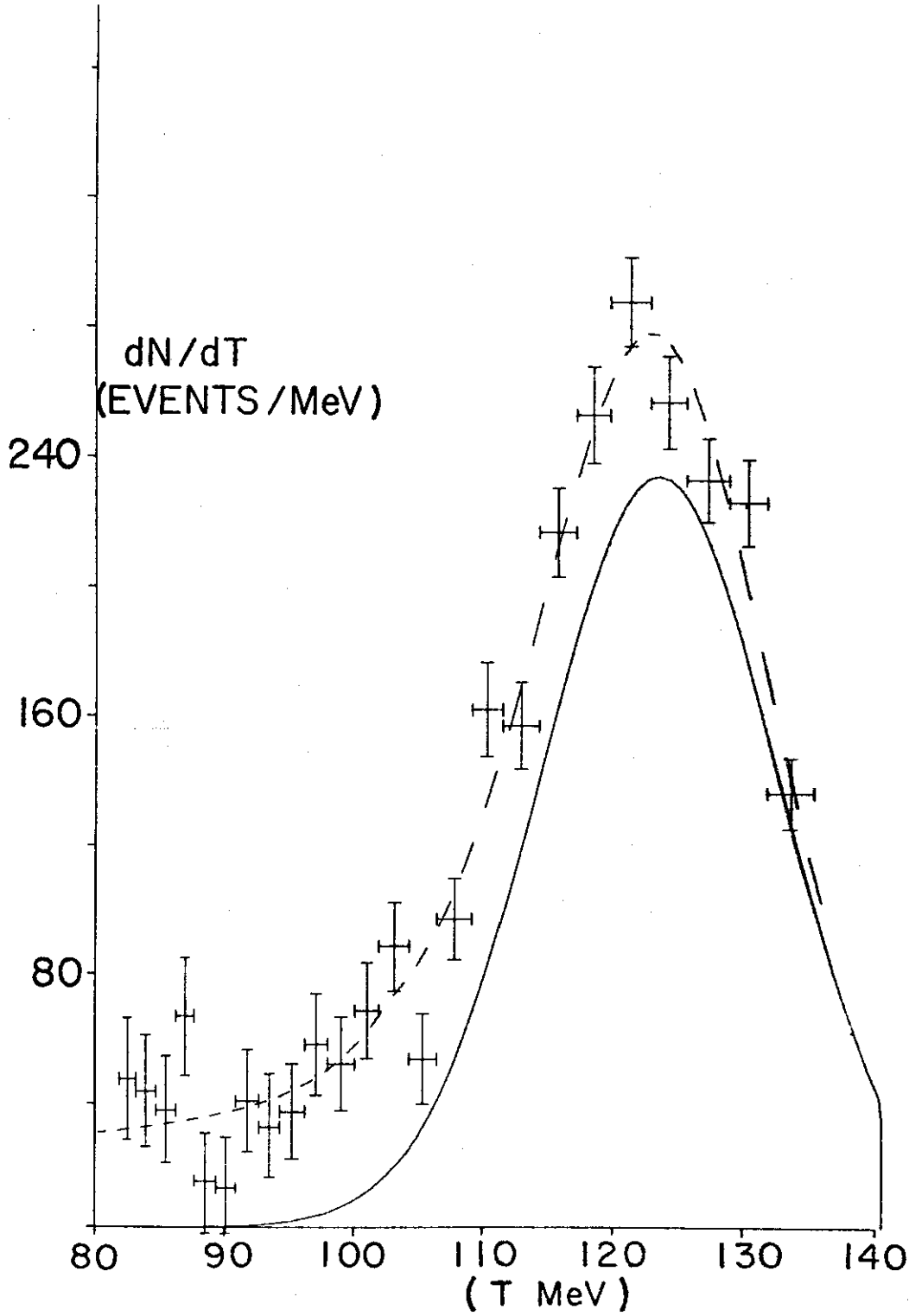
dN/dT
(EVENTS/MeV)
240
160
80
80
90
100
110
120
130
140
(T MeV)

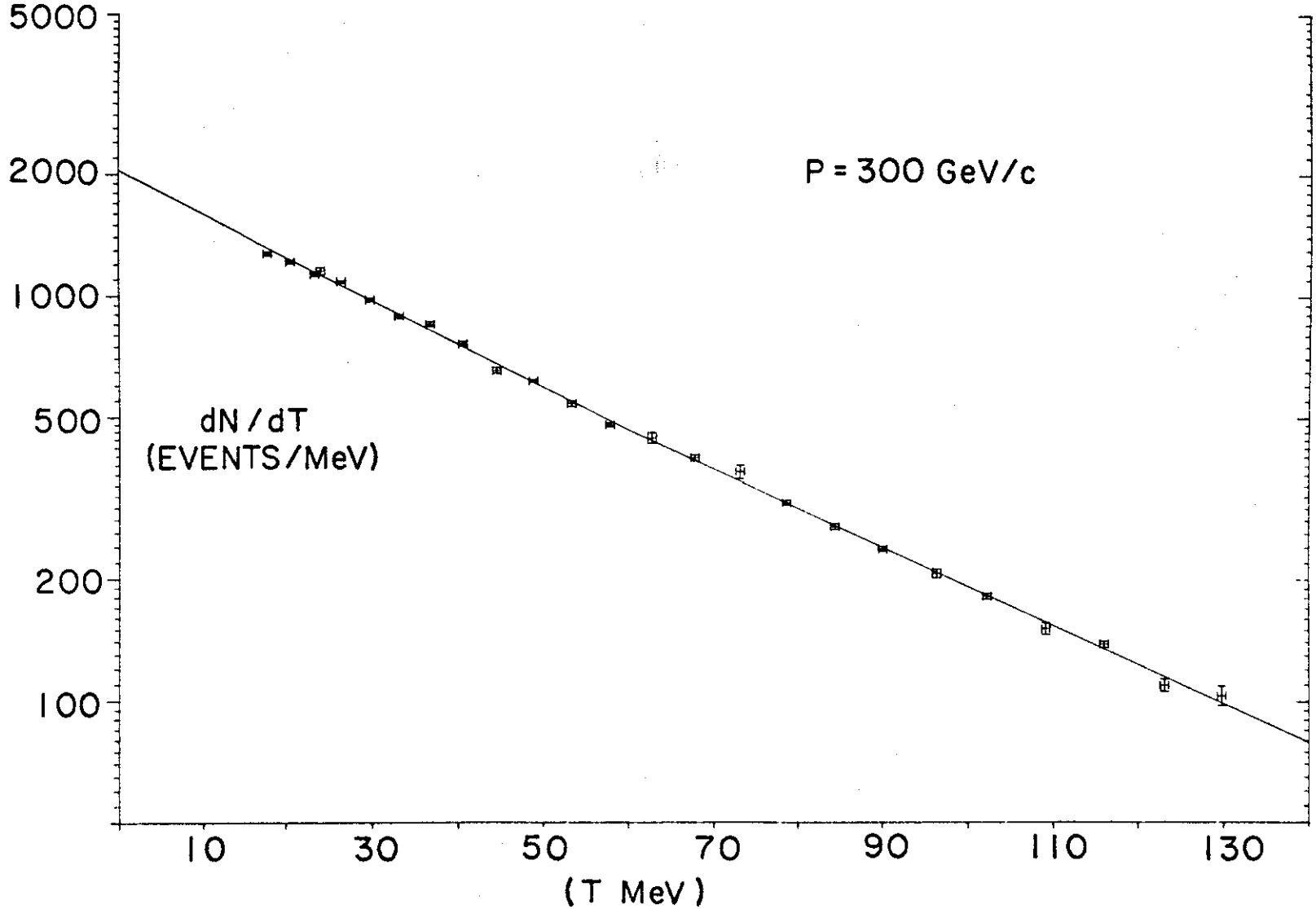
5000
2000
1000
500
200
100
P = 300 GeV/c
dN / dT
(EVENTS/MeV)
10
30
50
70
90
110
130
(T MeV)

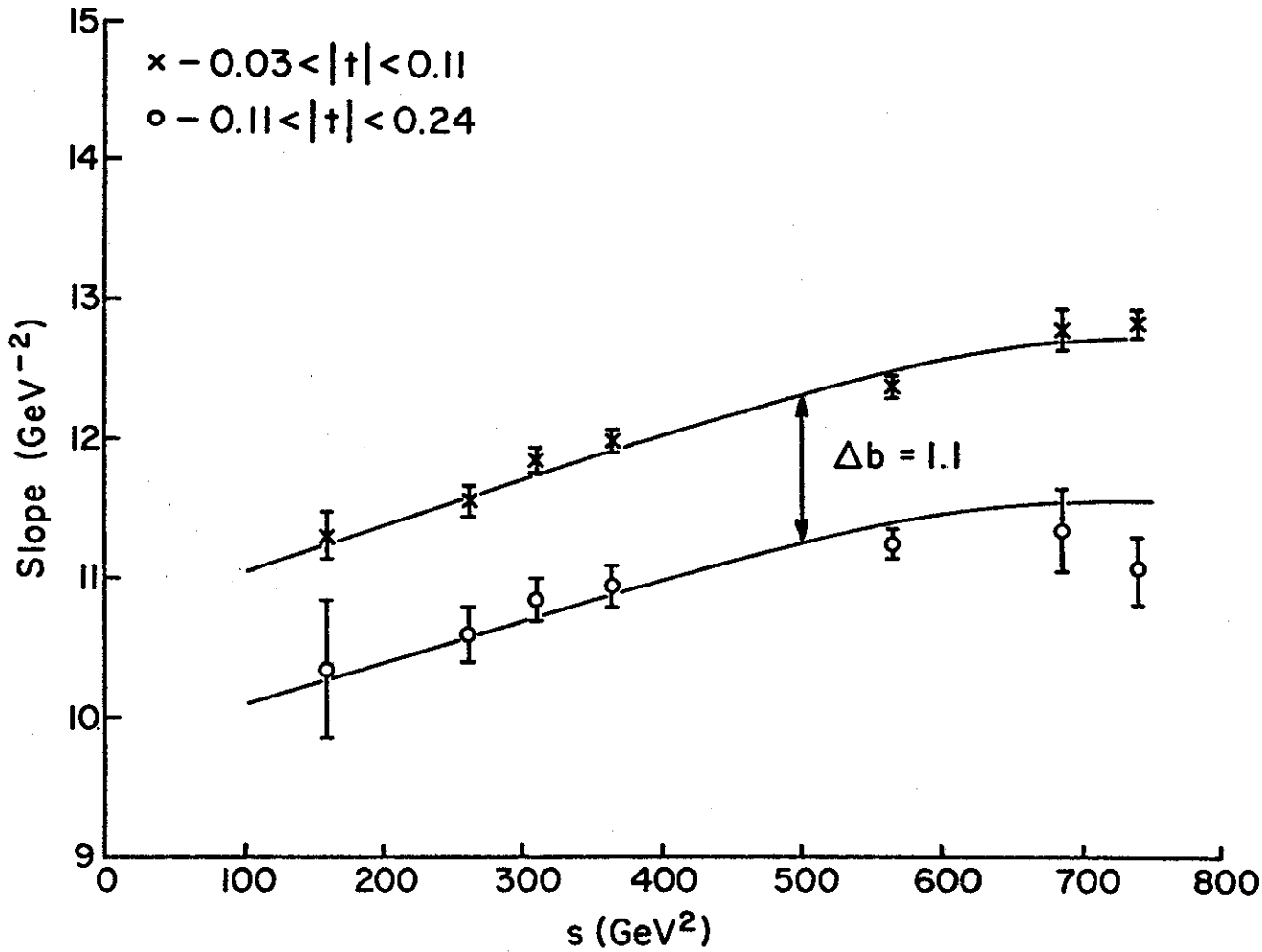
× – 0.03 < |t| < 0.11
o – 0.11 < |t| < 0.24
Δb = 1.1
Slope (GeV⁻²)
s (GeV²)
15
14
13
12
11
10
9
0
100
200
300
400
500
600
700
800

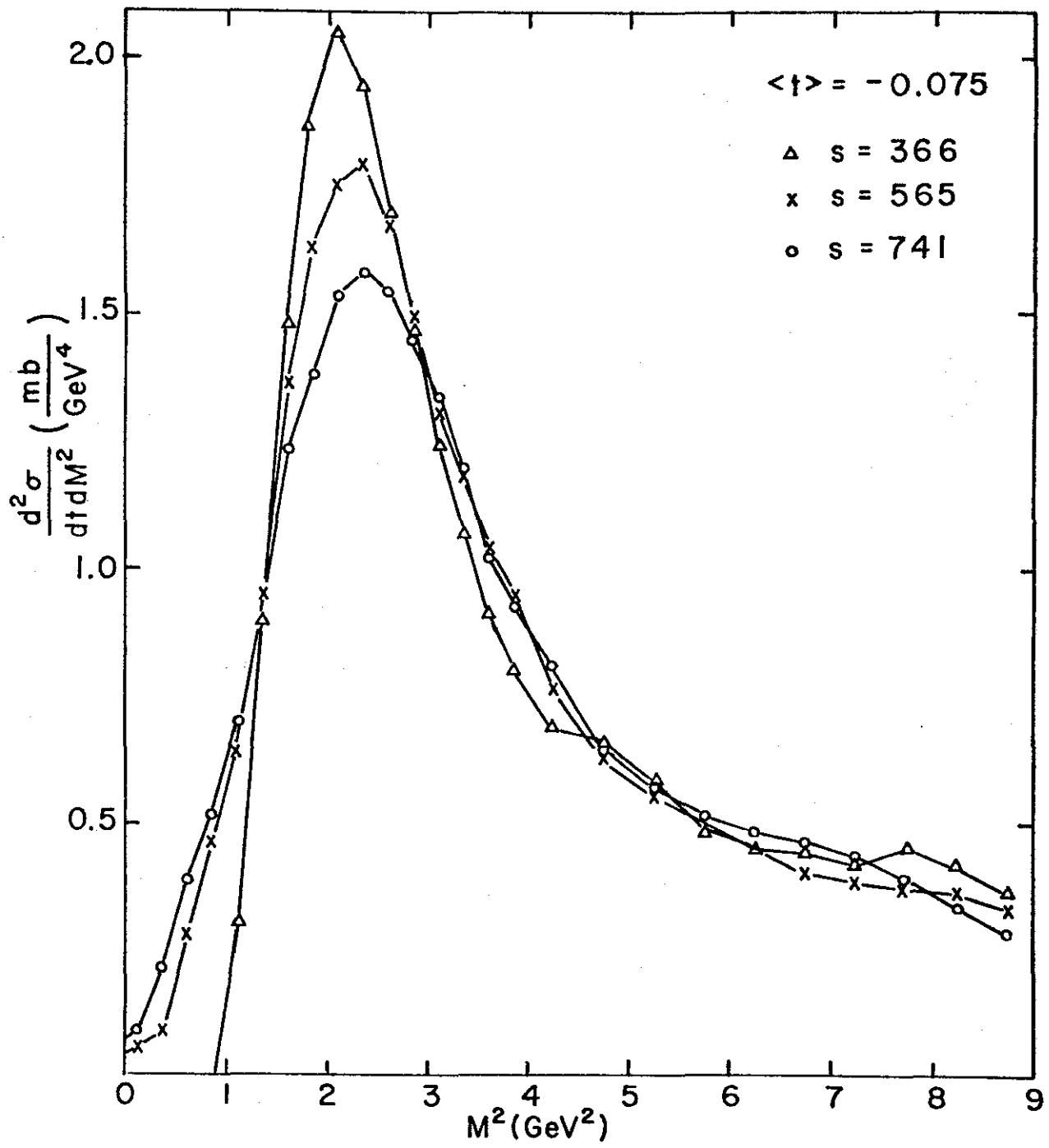
2.0
1.5
1.0
0.5
$\frac{d^2\sigma}{dt\,dM^2}\left(\frac{mb}{GeV^4}\right)$
<t> = -0.075
Δ s = 366
x s = 565
o s = 741
0
1
2
3
4
5
6
7
8
9
M^2 (GeV^2)

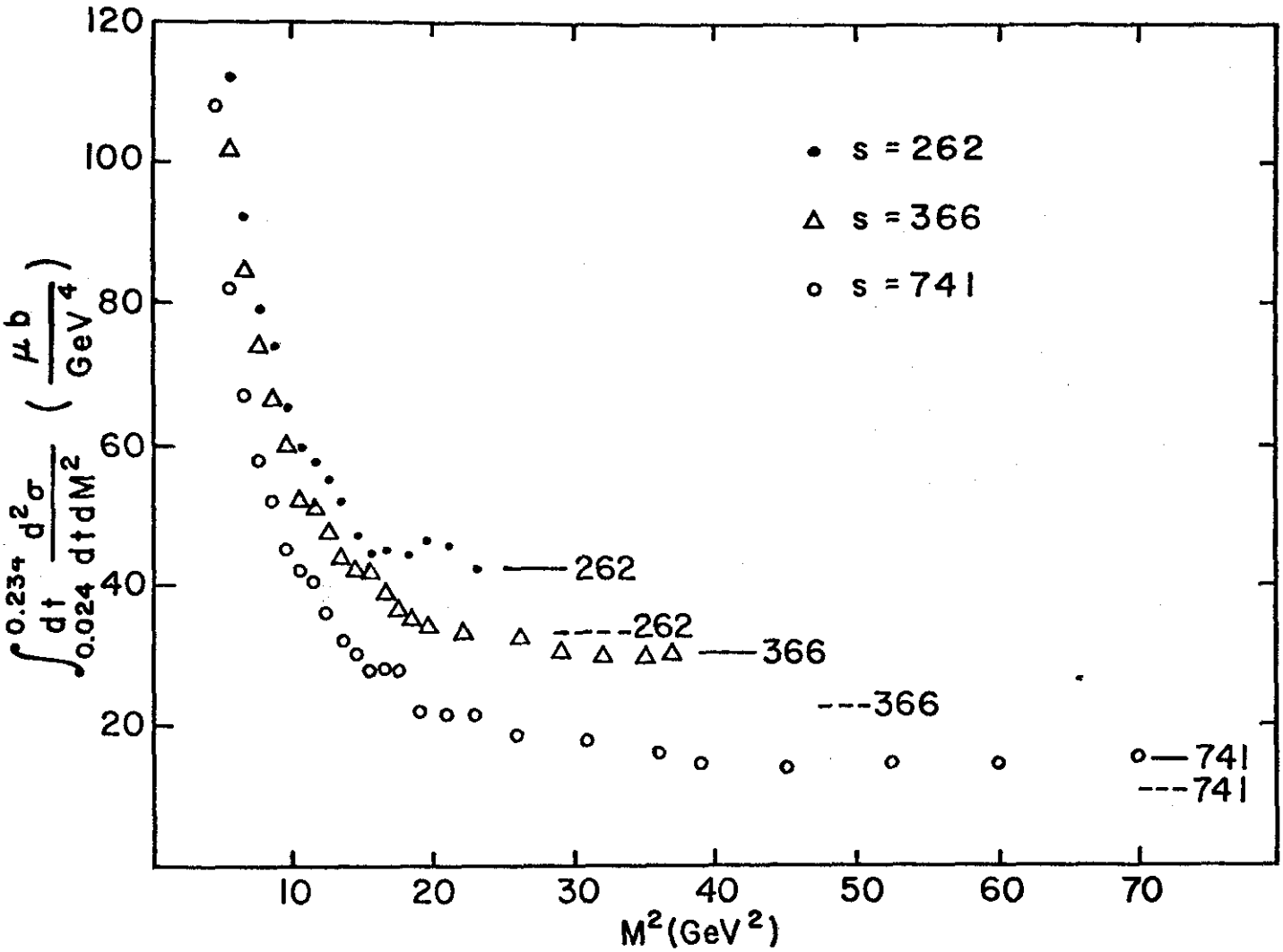
120
100
80
60
40
20
10
20
30
40
50
60
70
$M^2(GeV^2)$
$\int_{0.024}^{0.234} dt \frac{d^2\sigma}{dt\,dM^2} \left(\frac{\mu b}{GeV^4}\right)$
• s = 262
△ s = 366
○ s = 741
——262
----262
——366
---366
○—741
---741

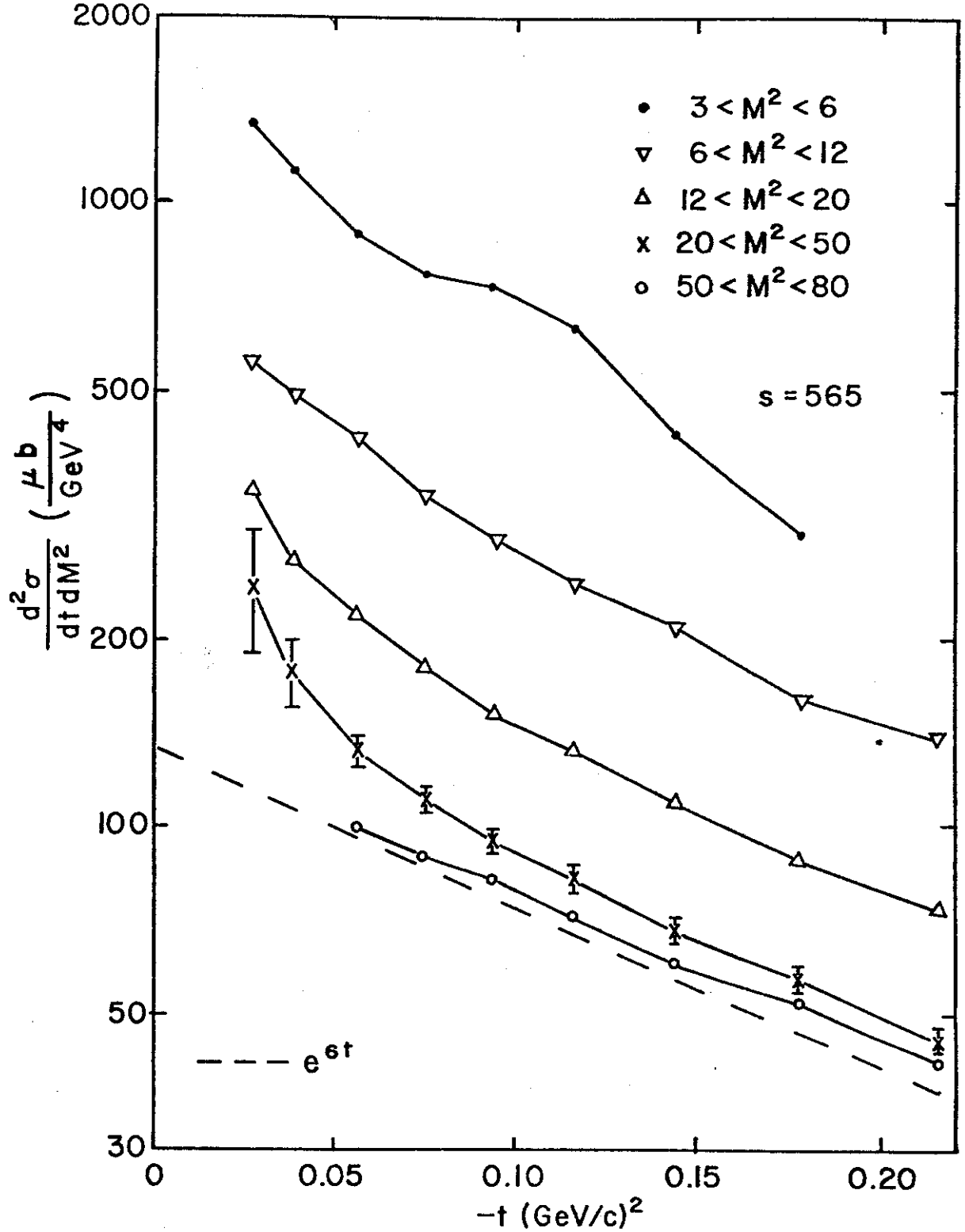
2000
1000
500
200
100
50
30
0
0.05
0.10
0.15
0.20
$-t$ (GeV/c)^2
$\frac{d^2\sigma}{dt\,dM^2}$ $\left(\frac{\mu b}{GeV^4}\right)$
$3 < M^2 < 6$
$6 < M^2 < 12$
$12 < M^2 < 20$
$20 < M^2 < 50$
$50 < M^2 < 80$
s = 565
e^{6t}

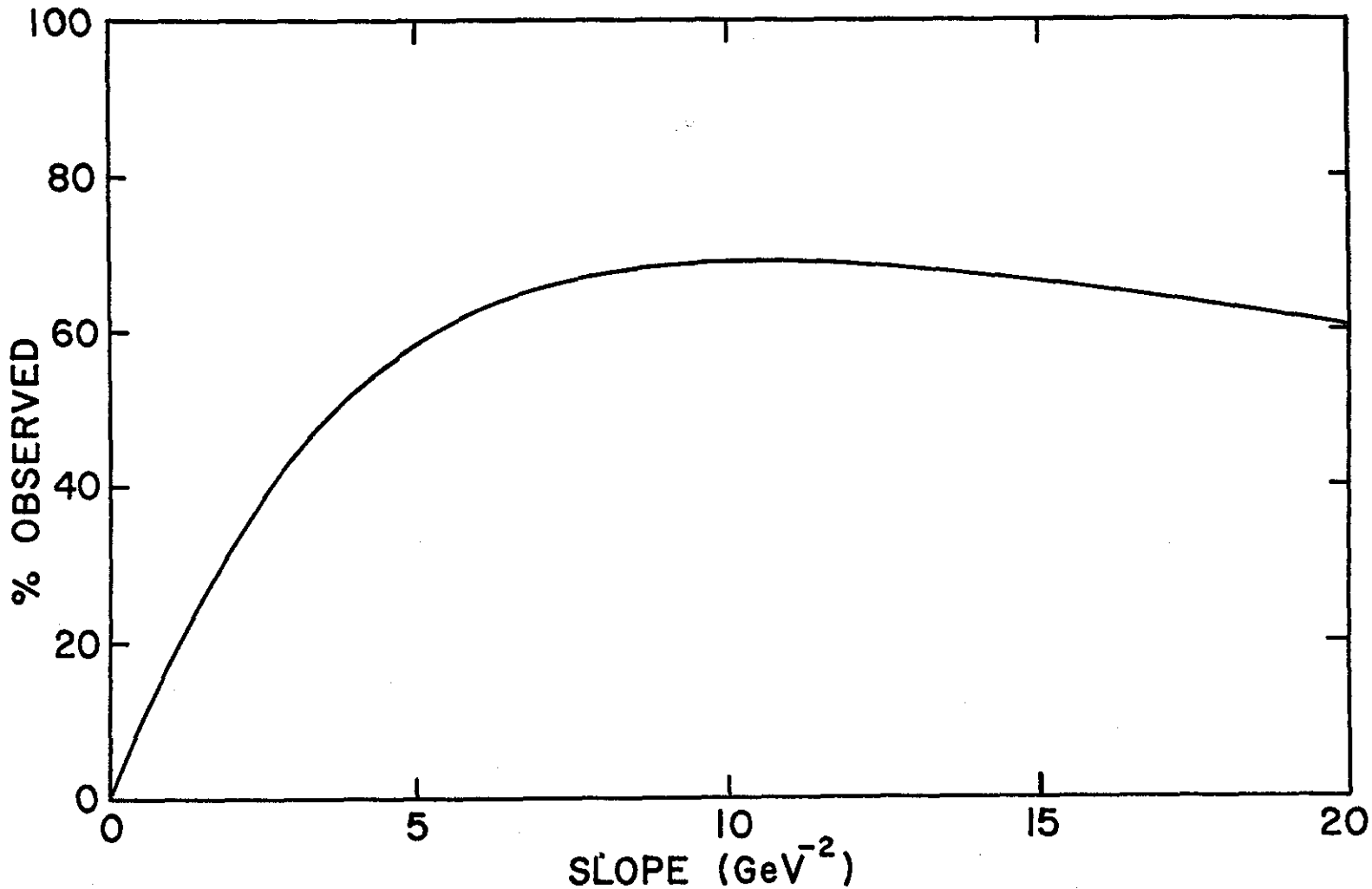
100
80
60
40
20
0
% OBSERVED
0
5
10
15
20
SLOPE (GeV^{-2})

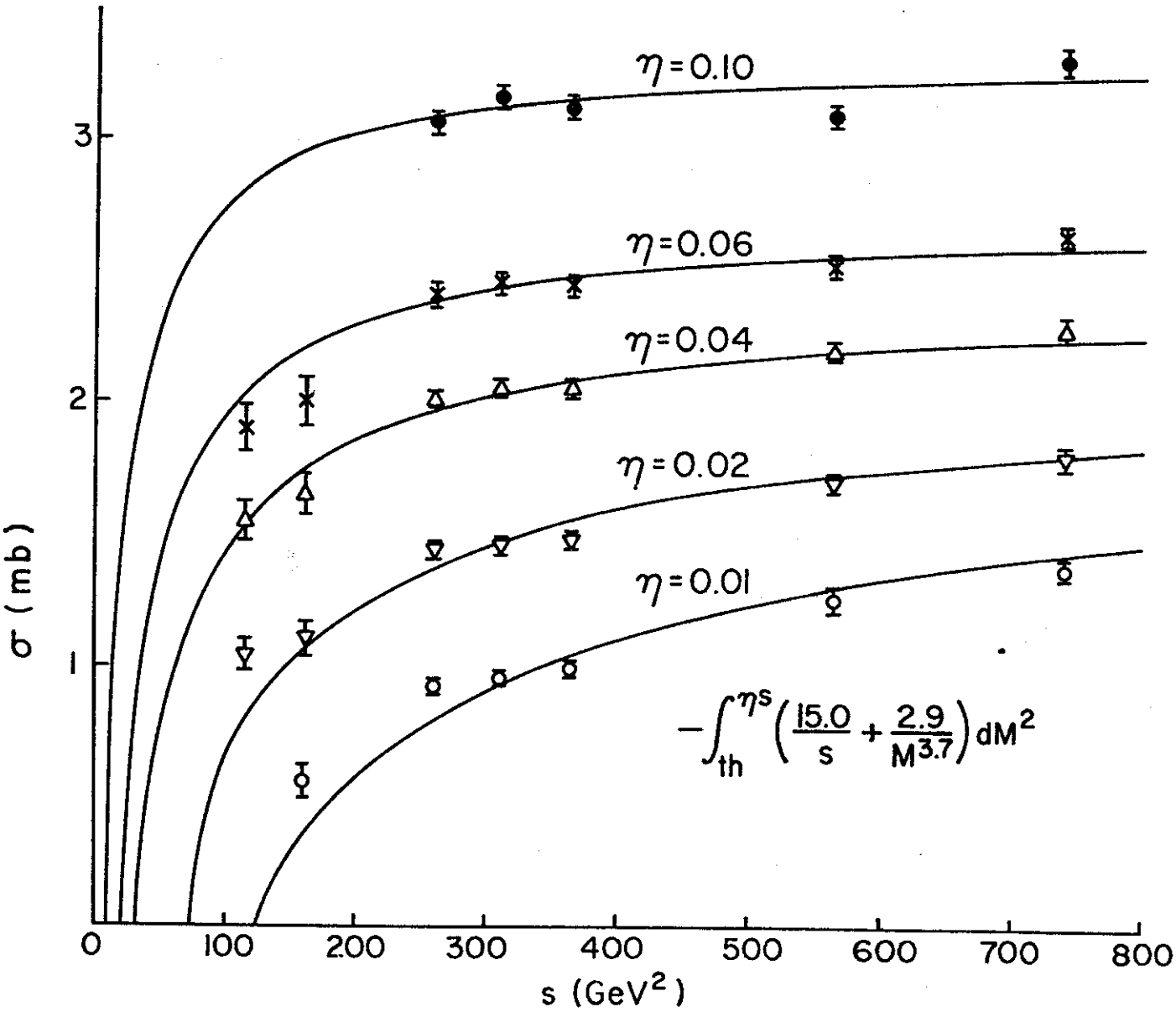
η = 0.10
η = 0.06
η = 0.04
η = 0.02
η = 0.01
$-\int_{th}^{\eta s}\left(\frac{15.0}{s}+\frac{2.9}{M^{3.7}}\right)dM^2$
σ (mb)
s (GeV²)
0
100
200
300
400
500
600
700
800
1
2
3

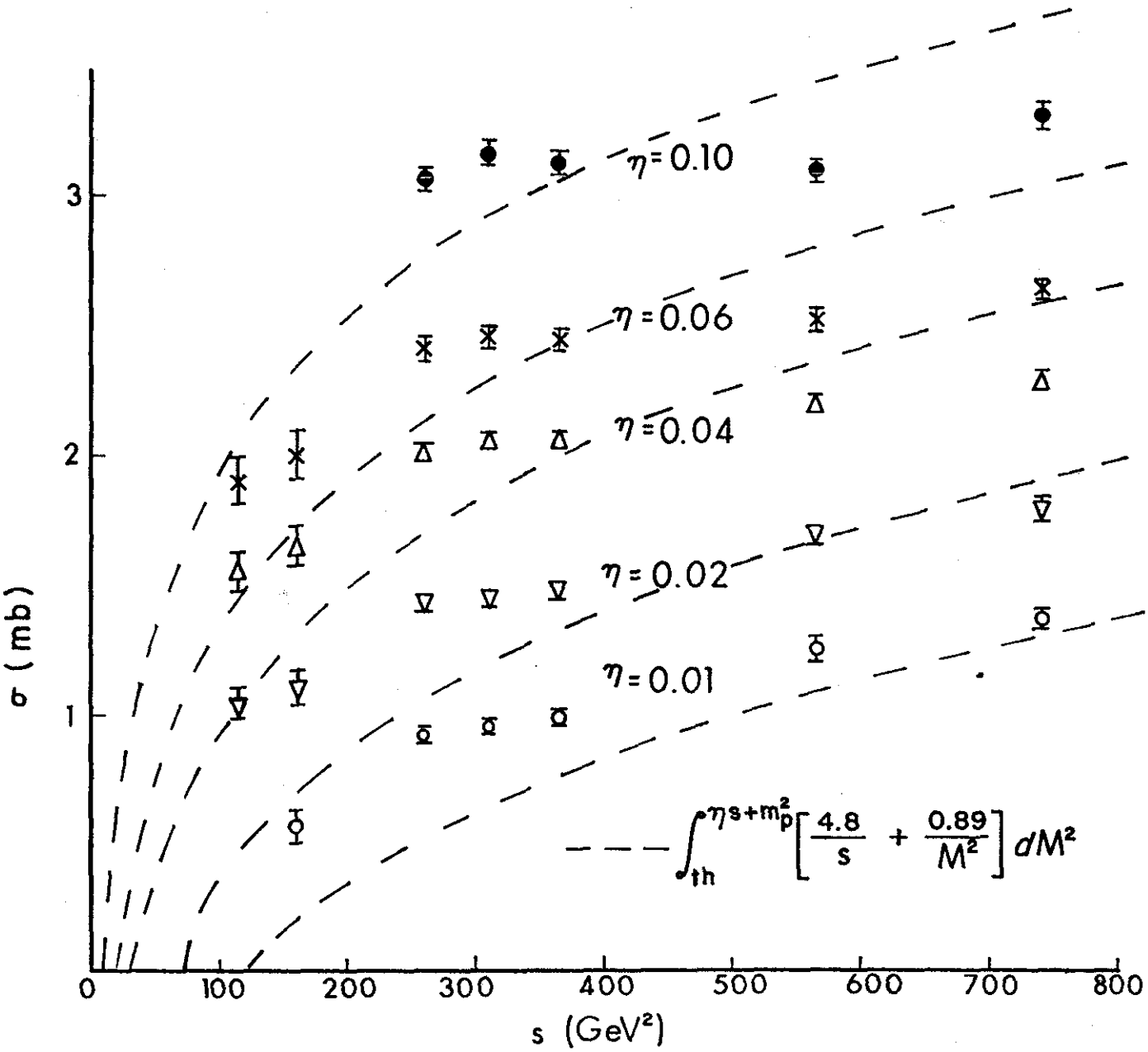
σ (mb)
s (GeV²)
η = 0.10
η = 0.06
η = 0.04
η = 0.02
η = 0.01
$\int_{th}^{\eta s+m_p^2}\left[\frac{4.8}{s}+\frac{0.89}{M^2}\right]dM^2$
0
100
200
300
400
500
600
700
800
1
2
3

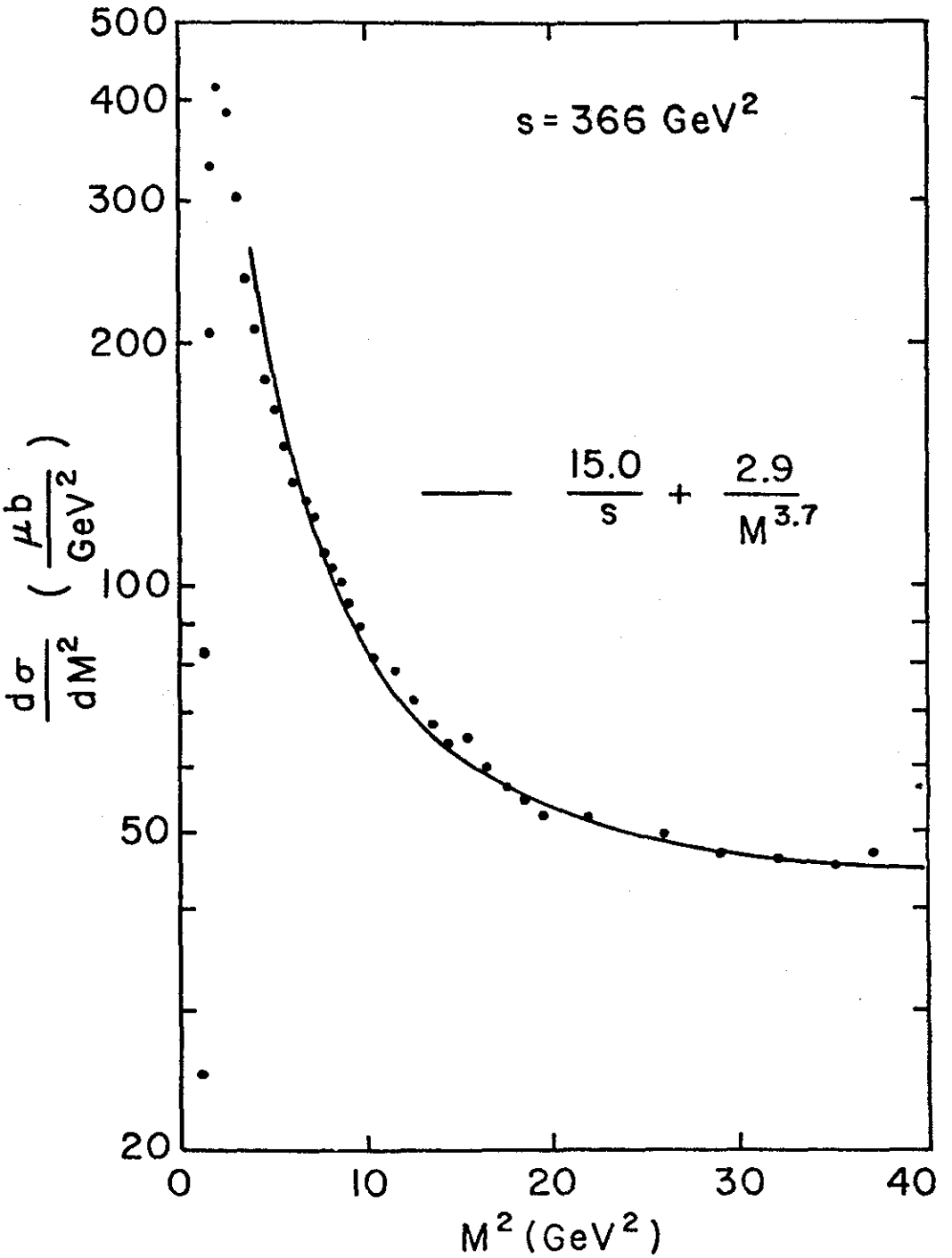
500
400
300
200
100
50
20
0
10
20
30
40
s = 366 GeV²
15.0/s + 2.9/M^3.7
dσ/dM² (μb/GeV²)
M² (GeV²)

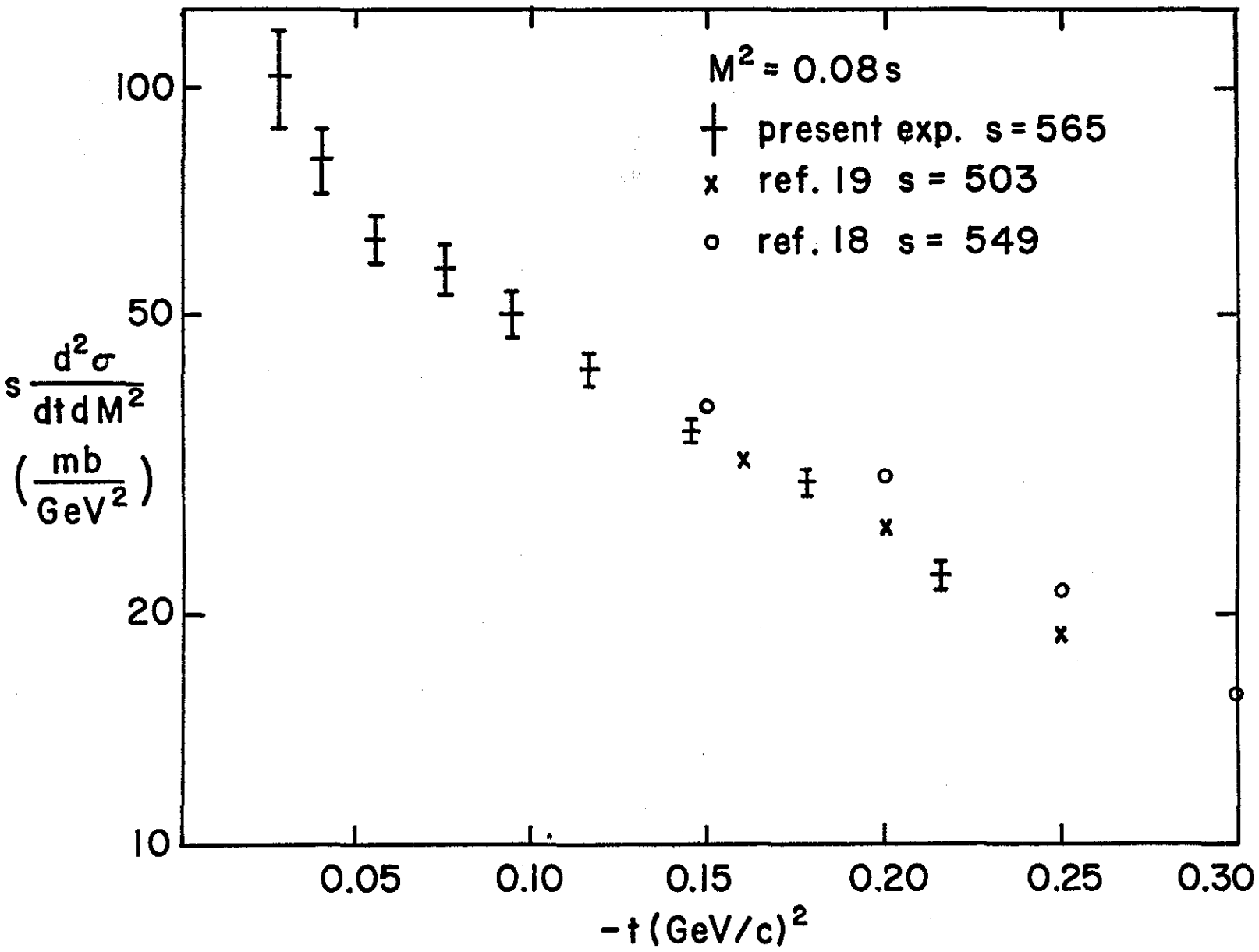
$M^2 = 0.08s$
present exp. s = 565
ref. 19 s = 503
ref. 18 s = 549
100
50
20
10
$s\frac{d^2\sigma}{dt\,dM^2}$
$\left(\frac{mb}{GeV^2}\right)$
0.05
0.10
0.15
0.20
0.25
0.30
$-t\,(GeV/c)^2$

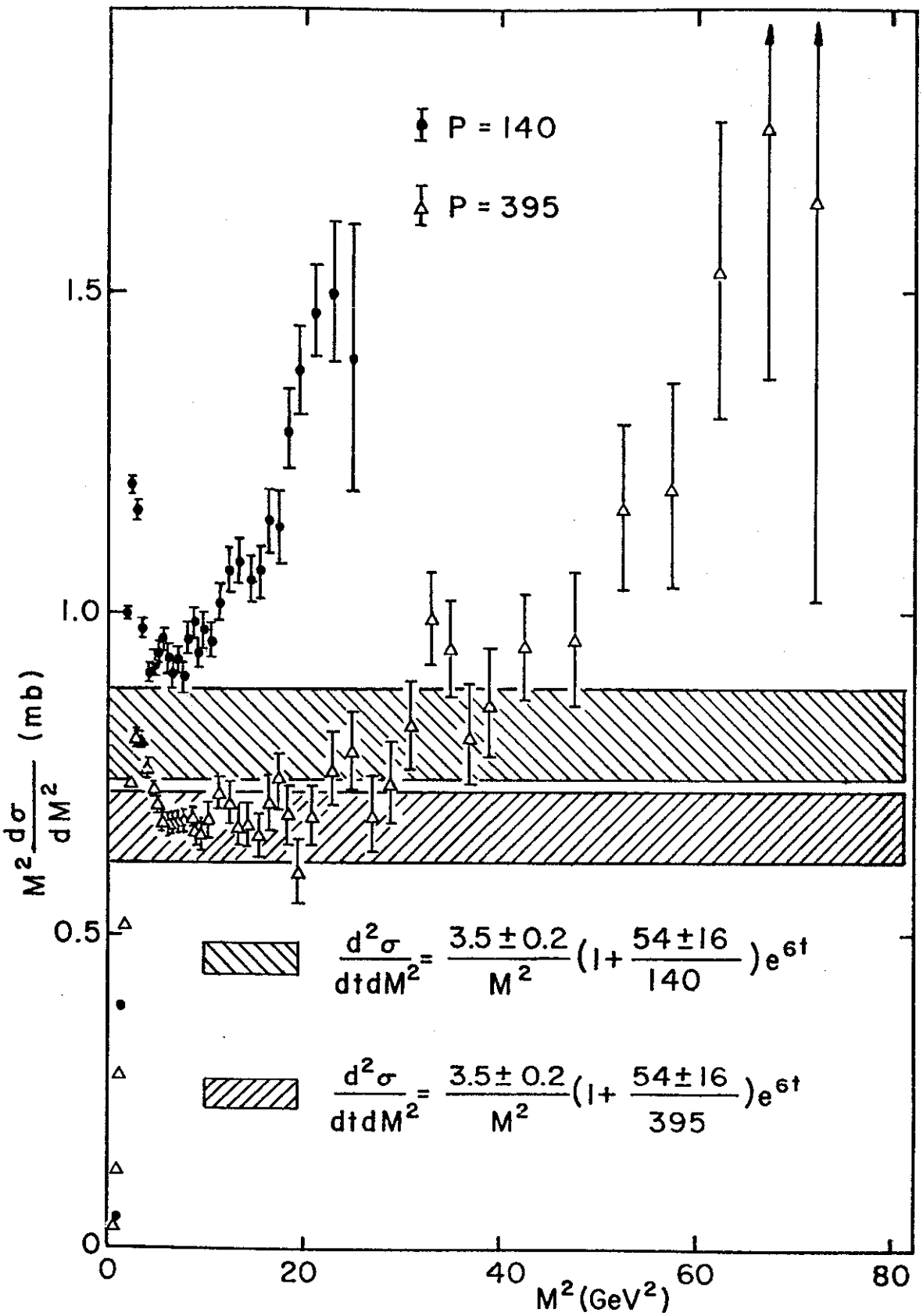
P = 140
P = 395
1.5
1.0
0.5
0
$M^2 \frac{d\sigma}{dM^2}$ (mb)
$\frac{d^2\sigma}{dt\,dM^2} = \frac{3.5 \pm 0.2}{M^2}\left(1 + \frac{54 \pm 16}{140}\right)e^{6t}$
$\frac{d^2\sigma}{dt\,dM^2} = \frac{3.5 \pm 0.2}{M^2}\left(1 + \frac{54 \pm 16}{395}\right)e^{6t}$
0
20
40
60
80
M^2 (GeV^2)